August 2020

Deterministic Model of the Voltage Dependent Anion Channel (VDAC) Kinetics

Viren Shah
University of Wisconsin-Milwaukee

DETERMINISTIC MODEL OF THE VOLTAGE DEPENDENT ANION CHANNEL (VDAC) KINETICS

by

Viren Shah

A Thesis Submitted in

Partial Fulfillment of the

Requirements of the Degree of

Master of Science

in Engineering

at

The University of Wisconsin-Milwaukee

August 2020

ABSTRACT

DETERMINISTIC MODEL OF THE VOLTAGE DEPENDENT ANION CHANNEL (VDAC) KINETICS

by

Viren Shah

The University of Wisconsin – Milwaukee 2020
Under the Supervision of Professor Ranjan Dash (Medical College of Wisconsin)

The voltage-dependent anion channel (VDAC) is a voltage gated channel residing on the outer mitochondrial membrane (OMM) that facilitates the flow of metabolites between the cytosol and mitochondria. The channel is regulated through conformational changes driven by electrostatic effects along with numerous regulatory mechanisms. The aim of this study is to mechanistically model kinetics of substrate flow through VDAC and incorporate them into existing mechanistic computational models of mitochondrial function. The resulting model is used in two ways: 1) to establish mitochondrial bioenergetics (conductance, permeability, and current/flux) under physiological conditions, and 2) to conduct perturbations simulating the effect of altered VDAC kinetics (resulting in altered membrane permeabilities and substrate fluxes) by cellular regulatory changes (such channel closure) on overall mitochondrial function.

TABLE OF CONTENTS

LIST OF FIGURES

LIST OF TABLES

1 Background

1.1 VDAC

Mitochondria are present in most eukaryotic cells and are characterized by having a double membrane. The inner mitochondrial membrane (IMM) contains many specialized channels and transporter proteins, while the voltage dependent anion channel (VDAC) is the primary channel on the outer mitochondrial membrane (OMM) (M. Colombini et al., 1996). VDAC is a relatively small pore forming protein, found to be highly conserved across species and found on all mitochondria. VDAC is abundantly found on the OMM, estimated to comprise of 50% of the overall OMM protein population (Shoshan-Barmatz et al., 2010). The function of VDAC is to regulate and facilitate the flow of metabolites between the cytosol and mitochondrial intermembrane space, and thereby providing a regulatory mechanism to control overall mitochondrial activity (M. Colombini, 1979; Mannella et al., 1990; Zambrowicz et al., 1993). This function is accomplished mainly by a gating mechanism which responds to changes in membrane potential and external regulators. These changes drive structural changes causing the channel to transition between various sets of closed and open states (M. Colombini, 1980). Figure 1 below demonstrates the characteristic function of VDAC in mediating metabolite flux. ATP flux is allowed at membrane potentials favoring an open channel state and blocked at membrane potentials favoring closure (T. Rostovtseva et al., 1997).

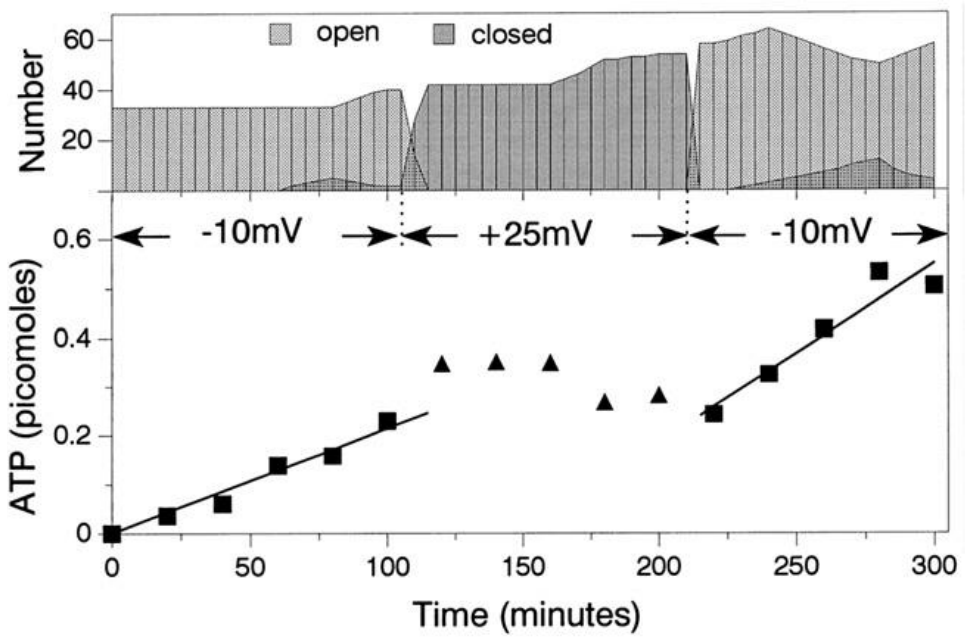

Figure 1: Study demonstrating the characteristic function of VDAC. ATP flux is present while channel is open, while closure blocks ATP flux through VDAC (T. Rostovtseva et al., 1997)

1.1.1 Structure

VDAC is made up of a single 30kDa polypeptide, which forms into a beta barrel structure with a single alpha helix (Mannella et al., 1990). Analysis of the polypeptide have determined 19 beta strands (alternating polar/non-polar amino acid patterns) (Bayrhuber et al., 2008; M. Colombini et al., 1996). There is experimental evidence that there exists a mobile α-helix on the N-terminal of the protein which is critical to its voltage sensing properties. This region is not attached to the barrel structures wall, however interacts with it via hydrogen bonds (R. Ujwal et al., 2008). Further experiments introducing point mutations on beta strands and the alpha helix present at the N-terminus show a loss of this functionality (Vito De Pinto et al., 2008). Figure 2 below demonstrates a cartoon depiction of the 19 beta strand structure (Choudhary et al., 2014; Geula et al., 2012).

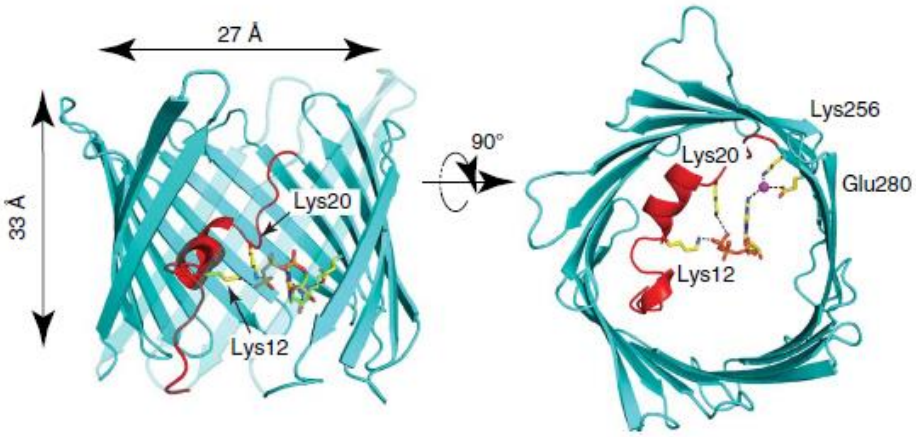

Figure 2: Representation of VDAC with β-barrel (cyan) and N-terminal α-helix (red) interacting with ATP molecule (Choudhary et al., 2014)

There is some controversy in literature whether the native folded structure of the protein wall consists of 19 beta strands (Hiller et al., 2010), with certain researchers favoring a 13 beta strand structure with the single α-helix within the barrel structure instead (M. Colombini, 2012a). Structures determined by NRM and X-ray diffraction from refolded VDAC proteins support a 19 beta strand model. Alternatively, experimental evidence based on introducing point mutations on the 19 beta strands demonstrate that 6 of the strands are apparently not critical to the structure and function of the channel (i.e. do not cause loss of voltage sensing functionality) and seem to support a 13 beta strand structure instead (Choudhary et al., 2014). These contradictions are yet to be fully resolved and it will be important to fully elucidate the mechanism by which the channel responds to changes in membrane potential via further research.

It has been demonstrated that both the C and N terminus of VDAC are oriented toward the mitochondrial inter-membrane space in their native conformations at zero membrane potentials (Kahle et al., 2013; Shoshan-Barmatz et al., 2010), however other experiments suggested VDAC is randomly oriented within the membrane (Marques et al., 2004; Rachna

Ujwal et al., 2014). The location of various residues and overall orientation of the structure are important in understanding its regulation and potential for therapeutic use.

1.1.2 Gating mechanism

VDAC gating process consists primarily of three sets of states (as depicted in Figure 3): two distinct sets of closed states at positive and negative membrane potentials, and an open state at low/zero membrane potentials. The open state is approximated to be ~2.5-3nm in diameter and closed states approximated to ~1.7-1.9nm in diameter (M. Colombini, 1980; M. Colombini et al., 1996; Hiller et al., 2010; Shoshan-Barmatz et al., 2010).

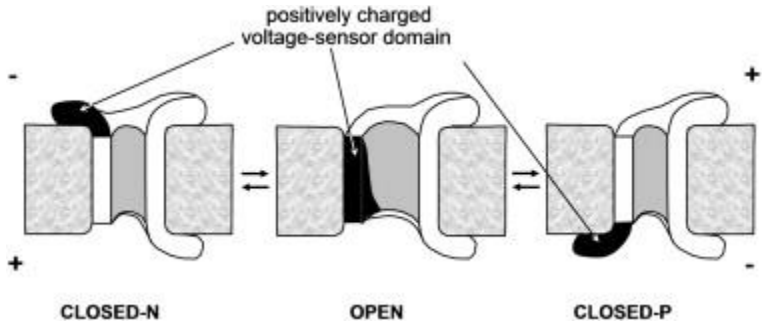

Figure 3: The voltage gating mechanism for VDAC from literature (from Colombini, 1996)

Generally, there is believed to be one open state of the channel sensitive to changes in membrane potential, and several possible closed states with varying sensitivity to voltage changes.[2] Experiments show that immediately after transitioning from open to closed states channels are easier to "reopen", however as the protein spends longer durations in elevated membrane potentials it transitions to lower conducting closed states and becomes more difficult to open once elevated potentials subside (M. Colombini et al., 1996).

1.1.2.1 Voltage sensor

The intriguing and unique characteristic of VDAC and its gating mechanism is the presence of a voltage sensing region which responses to changes in membrane potential to drive conformational changes in the protein. Studies of mutant VDAC proteins with single amino acid

substitutions indicate the voltage sensor forms part of the channel structure during the open state and helps facilitate anion flux. During the closed state, this portion is translocated out of the channel both constricting the channel and removing its anion selectivity (M. Colombini et al., 1996; Hiller et al., 2010). This is well depicted above in Figure 3.

1.1.3 Selectivity

The selectivity of the channel is based on both steric (size) and electrostatic restrictions, as well as being influenced by the overall three dimensional structure of the protein channel (i.e position of various amino acid side chains) in its interaction with individual molecules (M. Colombini, 2012b).

1.1.3.1 Steric restrictions

The steric restrictions of the channel are directly correlated to its pore size, which varies depending on the state (open or closed) the channel is in. For the open state, molecules with less than a 2.5nm diameter are theoretically able to permeate, corresponding to approx. 4000 Daltons. For the closed state, this reduces to a ~1.7nm diameter (Hodge et al., 1997; Mannella et al., 1990).

1.1.3.2 Electrostatic effects

While both cation and anions can pass through VDAC, the channel has been shown to be anion selective when open, and slightly cation selective while closed. This is driven by a combination of conformational changes (changes in pore size) and a difference in electrostatic effects on ionic species between the open and closed sets of stages of the channel (M. Colombini, 2012b).

The crude understanding of the channel is that when open, the charge on the channel walls is positive, thus making the channel anion selective. Upon interaction with elevated potentials across the membrane, the channel undergoes conformational changes, as discussed

prior, pushing a portion of the channel outward and altering the charge on the channel walls along with constricting its diameter. This effectively closes the channel to anion flux (T. Rostovtseva et al., 1997; Tatiana K. Rostovtseva et al., 1998; Zizi et al., 1998).. Flux of cations and relatively small uncharged substrates are shown to remain somewhat steady across the open and immediate closed states (lower closed states have not been studied well). Experiments by Hodge and coworkers shown below in Figure 4 demonstrate this behavior, wherein fluxes of common anions are significantly altered upon channel closure, however the same behavior is not observed with cations (Hodge et al., 1997).

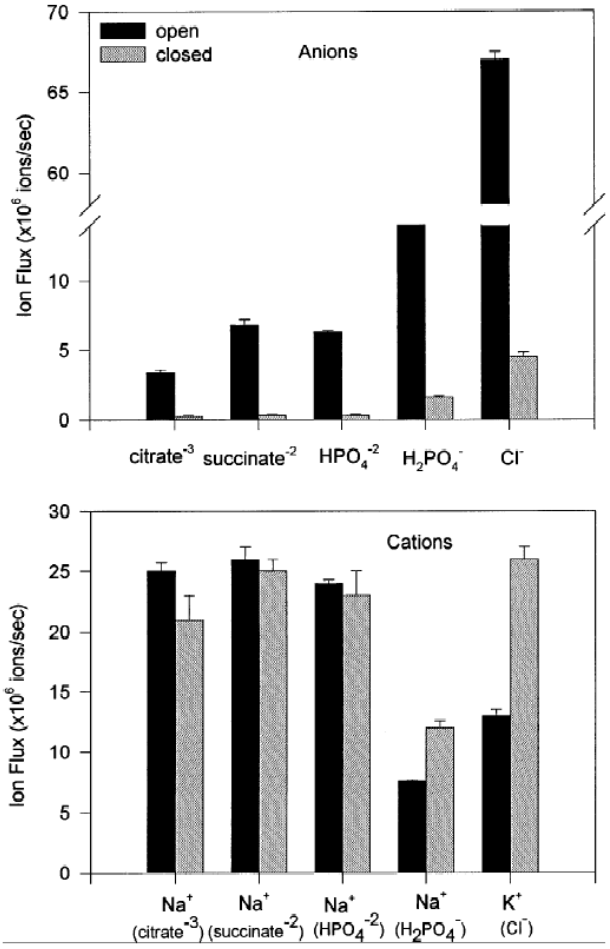

Figure 4: Anion and cation selectivity in VDAC open and closed states (from Hodge et al., 1997)

1.1.3.3 Channel effects

The major metabolites which need to be translocated across the OMM are ATP and ADP. Studies comparing similarly charged and sized molecules to ATP show that VDAC has a clear preference to promote the passage of ATP compared to other molecules. Considering its placement on the OMM and importance of ATP/ADP flux in maintaining cellular function, researchers propose the electrostatic and steric environment within the channel has evolutionally evolved to specifically facilitate ATP/ADP permeation. This behavior is evidenced by single channel permeability studies shown in Figure 5 below, which demonstrates that ATP (and its analog UTP) can permeate the channel while similarly sized and charged T-Glu or HPTS do not (T. K. Rostovtseva et al., 2002; M. G. Vander Heiden et al., 2000).

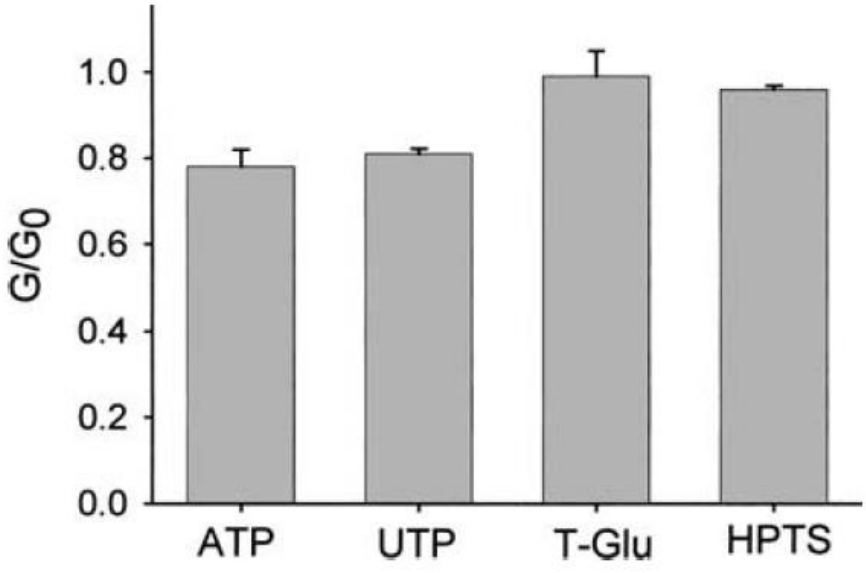

Figure 5: Single channel conductance of ATP (563 Da) and similarly charged, sized UTP (538 Da), T-Glu (581 Da), and HPTS (492 Da). VDAC shows selectivity for ATP and UTP but not toward molecules not found in normal mitochondrial function (T. K. Rostovtseva et al., 2002).

1.1.4 Metabolites

In addition to key substrates required for cellular respiration (ATP, ADP, inorganic phosphate) VDAC is the main pathway for all other metabolites exchanged between the mitochondria and cytosol.

The key metabolites, substrates and ions transported through VDAC are overviewed in **Table 1** below with their key properties and function.

Table 1. Key mitochondrial metabolites transported through VDAC

Metabolite Name	Function	Type	Negative / Positive	Charge	Net Flux	Primary Functions
ATP	**Product**	**Anion**	**Negative**	**-4**	**Out**	**Energy transfer**
ADP	**Substrate**	**Anion**	**Negative**	**-3**	**In**	**Substrate for energy metabolism**
AMP	**Substrate**	**Anion**	**Negative**	**-2**	**In**	**Substrate for energy metabolism**
Phosphate	**Substrate**	**Anion**	**Negative**	**-3**	**In**	**Substrate for energy metabolism**
Citrate	Substrate	Anion	Negative	-3	In	TCA cylce intermediate
Succinate	Substrate	Anion	Negative	-2	In	TCA cylce intermediate
Pyruvate	Substrate	Anion	Negative	-1	In	TCA cylce
alpha-Ketoglutarate	Substrate	Anion	Negative	-2	In	TCA cycle intermediate
aspartate	Substrate	Anion	Negative	-1	-	TCA cycle
Hydrogen (H+)	**Ion**	**Cation**	**Postive**	**1**	**-**	**Substrate for energy metabolism**
Calcium (Ca2+)	**Ion**	**Cation**	**Postive**	**2**	**-**	**Regulatory**
Sodium (Na+)	Ion	Cation	Postive	1	-	Regulatory
Potassium (K+)	**Ion**	**Cation**	**Postive**	**1**	**-**	**Volume homeostasis**
Magnesium (Mg2+)	Ion	Cation	Postive	2	-	Regulatory
***(BOLD in study)**						

1.1.5 Isoforms

VDAC has three genetic isoforms, named VDAC1, VDAC2, and VDAC3. These proteins are present in differing concentrations (with VDAC1 the most abundant) and perform distinct functions (Shoshan-Barmatz et al., 2010). Experimental data suggest that VDAC1 isoform (studied herein) is responsible for maintaining metabolite homeostasis between the intermembrane space and cytosol. Other two isoforms play critical yet poorly understood roles in mitochondrial development and homeostasis, and their effects on metabolite flux will not be studied herein (M. Colombini, 2012a).

In addition to VDAC isoforms localized on the OMM, differentially spliced VDAC isoforms have been found on other membranes as well. VDAC isoforms have been found on both the endoplasmic reticulum (ER), and sarcoplasmic reticulum (SR), and other cellular membranes (V. De Pinto et al., 2003; Gonzalez-Gronow et al., 2003). The precise functions of these extra-mitochondrial VDAC are not well studied in literature but are postulated to assist with nucleotide and metabolite transport akin to is primary role in the mitochondrial membrane (Shoshan-Barmatz et al., 2012).

1.1.6 Role in apoptosis

VDAC is a critical mediator for and against apoptosis. Under normal conditions, the outer membrane and VDAC are not permeable to proapoptotic proteins residing in the intermembrane space due to steric restrictions (M. Colombini, 2012a). These IMS proapoptotic proteins included cytochrome c (cyto c), apoptosis-inducing factor (AIF), and others. It is proposed that factors (both electrodynamic and protein induced effects) favoring open state VDAC conformations mediate against apoptosis by maintaining OMM permeability (McCommis et al., 2012). Proapoptotic factors have been shown to induce VDAC closure leading to a cascade of events resulting in IMM permeabilization and either the formation of various channels and complexes to release apoptotic proteins into the cytosol or otherwise inducing OMM rupture (Shoshan-Barmatz et al., 2010). Figure 6 overviews this signaling network.

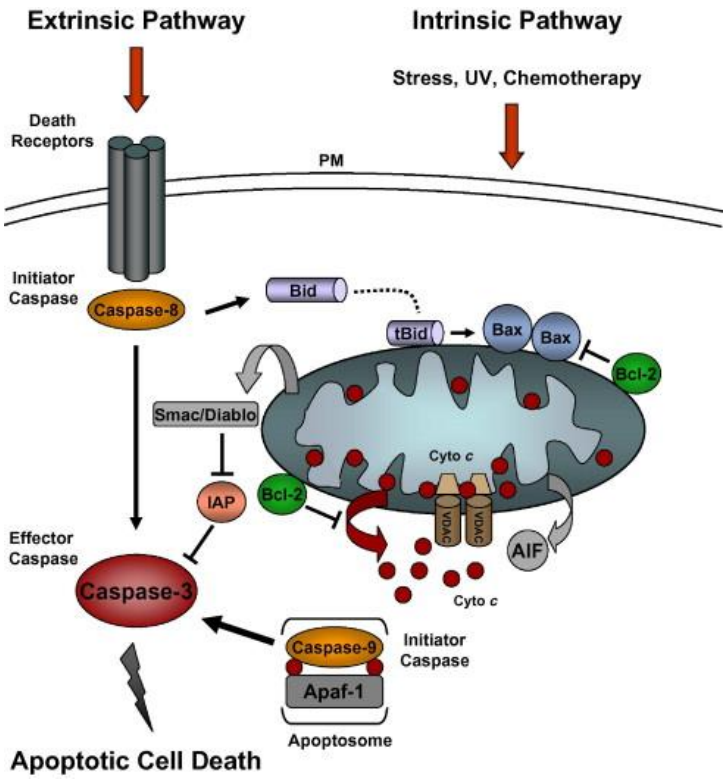

Figure 6: Various pathways in the apoptosis network. VDAC is a critical mediator for and against the release of cyto c driven by various signaling events (Shoshan-Barmatz et al., 2010)

This model is summarized in Figure 7 below. VDAC in an open state allows the for exchange of ATP/ADP through the OMM and IMM, and various factors including low OMM potential and other protein factors favor this anti-apoptotic state. When VDAC enters a closed state, this exchange is terminated and results in a environment favoring release of cyto C and initiation of apoptosis. Thus, VDAC acts as a switch like mechanism through which apoptosis can either be triggered (through factors favoring channel closure) or prevented (through factors favoring an open channel) (Crompton, 1999; T. K. Rostovtseva et al., 2008). The specific mechanisms at play in the IMS and matrix which lead to the permeation of the IMM and OMM are yet to be elucidated.

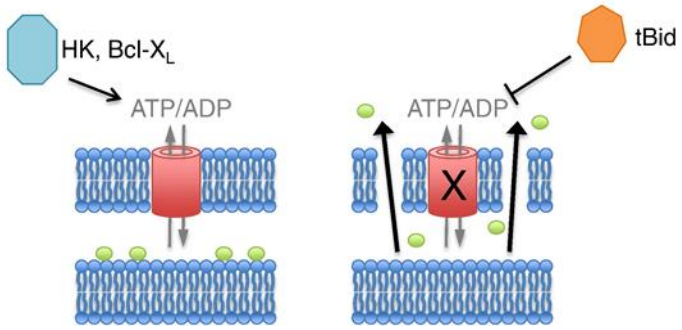

Figure 7: VDAC mediation of apoptosis via release of cyto c (partly adapted from McCommis et al., 2012)

1.1.7 Regulation and modulation

With the characteristic method of VDAC modulation having been discussed in detail (voltage driven conformational changes), this subsection focuses on additional pathways which alter VDAC states and change its properties.

As the primary gatekeeper for interactions with the mitochondria, VDAC is regulated by a variety of molecules and proteins to influence overall mitochondrial and cellular behavior. Certain pathways favor cellular growth and homeostasis or alternatively protect against apoptosis by maintaining open state VDAC conformations, while others induce closure and lead to either necessary apoptosis or dysregulation of cellular function. The next sections overview well established regulators and modulators of VDAC behavior, split by naturally occurring regulators and those which have been found to impact VDAC but have no known biological significance. **Table 2** provides a high-level overview.

1.1.7.1 "Natural" regulators

One of the main regulators of VDAC function are pro- and anti- apoptotic proteins from the Bcl-2 family. These proteins play a central role in controlling apoptosis, and mediate VDAC permeability to either favor or protect against it (T. K. Rostovtseva et al., 2008). Pro-apoptotic Bax, Bak, and tBid have been shown through various experimentation to insert into lipid membranes (such as the OMM), where they attach to VDAC and induce channel closure which

favors the aforementioned cascade. Anti-apoptotic proteins in this family such as Bcl-2 and Bcl-xL are shown to have opposite affects (Shimizu et al., 1999), helping maintain homeostasis by impeding the generation of OMM potential (Matthew G. Vander Heiden et al., 1997). Dysregulation of these anti-apoptotic proteins and by association OMM permeability has been shown to contribute to the development of tumors and ineffectiveness of certain chemotherapies (Shoshan-Barmatz et al., 2010).

Hexokinases are also key regulators of VDAC function. Hexokinase acts as a catalyst in the first step of glycolysis and are abundant in the cytosol. Both hexokinases isoforms (HK1 and HK2) bind with VDAC and inhibit other interactions (such as binding of Bcl-2 proteins) and thus apoptosis. Binding of hexokinases with VDAC prevents channel closure (McCommis et al., 2012). This binding is reversible and beneficial when cells are at homeostasis. Hexokinases are found to co-localize with VDAC and promote glycolysis by directly receiving ATP as it is produced in the mitochondria. However, glycolysis activity is high in many malignant cancer cells which leads to hexokinase being overexpressed and the prevention of necessary apoptosis (Shoshan-Barmatz et al., 2010).

Tubulin has been shown to be another key factor which promotes closure / blockage of VDAC. Tubulin bind directly with VDAC through penetration into the channel and reduction of its electrostatic properties. Tubulin, which is also a reversible inhibitor of VDAC, completes with hexokinase to favor a pro-apoptotic environment in the cell. Tubulin is increased when energy metabolism is decreased to promote apoptosis, while hexokinase is more active in homeostatic cells and cancer cells (Tatiana K. Rostovtseva et al., 2008; Saks et al., 2010).

Table 2. VDAC regulators

Protein / molecule / compound	Type	Pro- or anti apoptotic	Channel State	Proposed Mechanism	Reference
Actin	Cytosolic protein	Pro-apoptotic	Favors closed channel state	Reduces potential required for VDAC closure	(Xu et al., 2001)
Anti-apoptotic Bcl-2 family proteins (ex. Bcl-XL)	Cytosolic protein	Anti-apoptotic	Favors open channel state	Interactions with VDAC preventing change in membrane potential and closure	(Shimizu et al., 1999)
Ca^{2+} (calcium ions)	Ion	Pro-apoptotic	Favors closed channel state	VDAC is shown to have Ca^{2+} binding sites, and overload of calcium ions induces closure	(Tan et al., 2007)
DIDS	Compound	Anti-apoptotic	Blocks permeability of channel	DIDS binds with VDAC and blocks permeation through the channel	(Shoshan-Barmatz et al., 2010)
Hexokinase	Cytosolic protein	Anti-apoptotic	Favors open channel state	Co-localization with VDAC preventing channel closure	(Neumann et al., 2010)
Lipid regulators	Membrane lipids	Pro-apoptotic	Favors closed channel state	Reduces potential required to induce conformational changes in VDAC and induce closure	(Tatiana K. Rostovtseva et al., 2006)
NADH	Cytosolic protein	Pro-apoptotic	Induces closure	Interacts directly with VDAC	(Lee et al., 1996)
Pro-apoptotic Bcl-2 family proteins (ex. tBid, Bax, Bim, Bak)	Cytosolic protein	Pro-apoptotic	Induces irreversible closure	Interactions with OMM and VDAC inducing closure	(T. K. Rostovtseva et al., 2008; Shimizu et al., 1999)
Tubulin	Cytoskeletal protein	Pro-apoptotic	Induces closure	Binds with VDAC and blocks channel	(Tatiana K. Rostovtseva et al., 2008)

(partly adapted from T. K. Rostovtseva et al., 2008)

1.1.7.2 "Artificial" regulators

DIDS can be used to block VDAC. Blockage of VDAC using DIDS prevents permeation of metabolites through (either from the OMM into the IMS or visa versa) the channel and acts as a method to stop mitochondrial activity. DIDS also prevents the binding of pro-apoptotic proteins like Bcl-2 family protein Bax, and prevents cyto c release from the IMS (Shoshan-

Barmatz et al., 2010). Thus, while DIDS inhibits VDAC activity, it also has anti-apoptotic effect due to is prevention of cyto c release. This allows for an useful mechanism to study VDAC and overall mitochondrial behavior in various experimental environments (Liu et al., 2008). Other regulators of VDAC include ruthenium red (RuR) and Koenig's polyion (Shoshan-Barmatz et al., 2010), both of which are shown to inhibit VDAC function and protect against apoptosis.

1.1.7.3 Post-translational modifications (PTMs)

Post translation modifications (PTMs) to VDAC regulate its properties and can promote either pro- or anti-apoptotic environments. This occurs through changes in its bioenergetics and affinity to binding the various regulators discussed prior. There are numerous residues on VDAC documented in literature which can undergo various PTMs, with reversible phosphorylation and protein acetylation being the most well studied (Kerner et al., 2012). Certain modifications have been shown to inhibit VDAC degradation and increase its expression leading to an environment favoring cell death (Yuan et al., 2008). Other modifications, such as those driven by hexokinases have an opposite effect and protect against apoptosis (Chen et al., 2014). The précises signaling events and changes in mitochondrial biogenetics which arise as a result of PTMs have not been well studies and are yet to be elucidated.

1.1.8 Role in disease

There are no known diseases associated directly with VDAC mutations and/or arising malfunctions. Certain observed cases of VDAC deficiency and malfunction are linked to well known mitochondrial pathologies (such as Pearson's disease) wherein overall mitochondrial dysfunction may lead to reduced VDAC protein synthesis (M. Colombini, 2012b; Das et al., 2012). However, as discussed in the previous section VDAC does play a major role in the regulation (and dysregulation) of cell death. Through its mediation of apoptosis, dysregulation of VDAC is a component of many diseases. Select well characterized examples are provided below.

As a central regulator of apoptosis VDAC dysregulation has been studied and implicated in many more conditions (Shoshan-Barmatz et al., 2010).

1.1.8.1 VDAC in cancer

The aforementioned Bcl-2 family of anti-apoptotic proteins have been associated with the development of cancer by alteration of OMM permeability and preventing cell death mediated through VDAC closure. Additionally, promotion of mitochondrial mediated apoptosis through release of cyto c/caspase-9 is a major pathway of many anti-cancer therapies (Shoshan-Barmatz et al., 2012). Overexpression of both Bcl-2 family and HK proteins have been associated with drug resistance in cancer therapies (Fang et al., 2018). As such, inhibition of these interactions and promotion of VDAC closure both offer targets of cancer therapy.

1.1.8.2 VDAC in myocardial disease

Apoptotic signaling events in myocardial ischemia and reperfusion injuries have been shown to involve VDAC. The p38 MAP kinase pathway results in VDAC mediated apoptosis, and disruption of this pathway has been demonstrated to have a protective effect (Schwertz et al., 2007). Inhibition of VDAC interactions with regulatory agents present in this pathway provide a possible target to treat these diseases.

1.2 Mitochondria and VDAC

This section aims to overview key mitochondrial functions, with commentary on how they are regulated or impacted by changes to VDAC properties where appropriate. Energy metabolism in the mitochondria is composed of the tricarboxylic acid cycle (TCA), oxidative phosphorylation (OXPHOS) and the electron transport chain (ETC), and associated substrate transport. Each substrate, intermediate, and product is involved in the regulation of the overall process both directly through allosteric regulation of involved enzymes, as well as indirectly through bioenergetic constraints (Beard, 2005).

Figure 8 below summarily represents the key processes present (Dash, unpublished). The TCA cycle is depicted by reactions 1-11. OXPHOS and ETC are shown by complex I (CI), complex III (CIII), complex IV (CIV), F_oF_1-ATPase, and succinate dehydrogenase. The flow of key metabolites across the membranes is also depicted, occurring through specialized transported on the IMM, or through VDAC on the OMM.

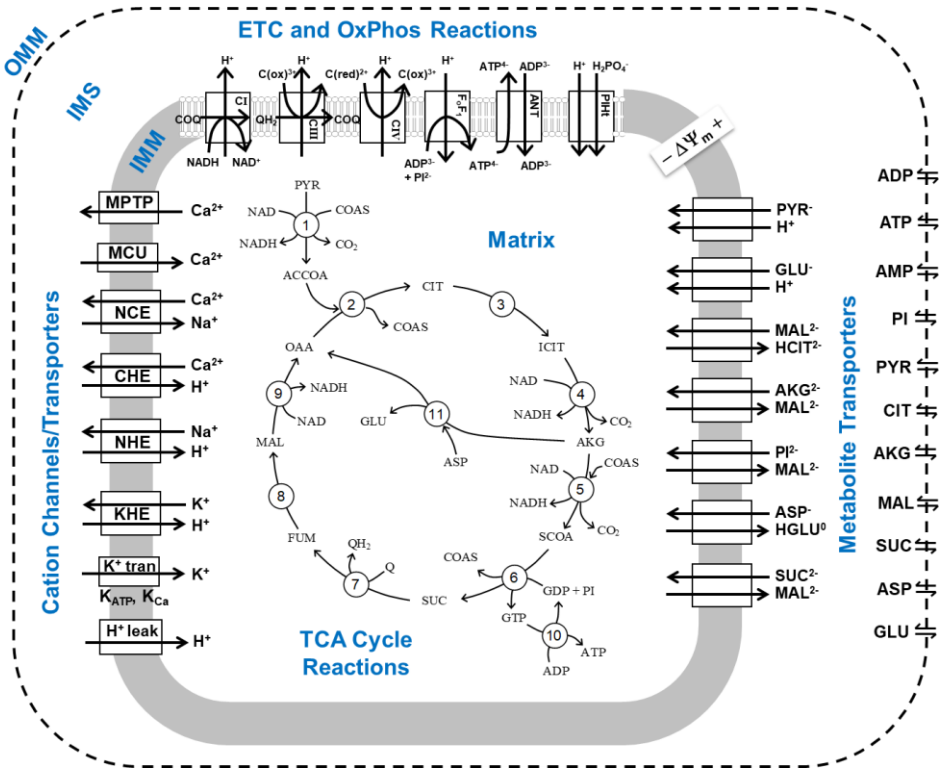

Figure 8: Illustration of key mitochondrial processes (Dash, unpublished)

1.2.1 Aerobic cellular respiration

1.2.1.1 TCA Cycle

The TCA cycle (also referred to as the Krebs cycle or the citric acid cycle) is composed of a series of reactions which release energy stored in pyruvate molecules produced in glycolysis. Prior to the cycle pyruvate is transported across both the OMM and IMM and is then converted to acetyl-CoA by pyruvate dehydrogenase in the mitochondrial matrix. Acetyl-CoA, in the presence of oxygen, undergoes a series of reactions which results in the production of

oxaloacetate (to be reused in future TCA cycles), 3 NADH, 1 $FADH_2$, and 1 GTP (or ATP upon conversion). In terms of the yield of one original molecule of glucose consumed in glycolysis (producing two pyruvates), the cycle repeats twice, and the products are doubled. NADH and $FADH_2$ are utilized further in the ETC to produce additional ATP via OXPHOS (Fall, 2002; Palmeira et al., 2012).

1.2.1.2 ETC and OXPHOS

The ETC uses products from the TCA cycle to drive OXPHOS and ATP production. Complex I – IV consume the products of the TCA cycle to create a proton gradient, which then utilized in complex V to produce ATP. Adenine nucleotide translocase (ANT) and phosphate translocase provide the necessary reagents (ADP, phosphate) and ANT also transfers produced ATP into the IMS. Each of the major processes are summarized below (Fall, 2002; Palmeira et al., 2012).

1.2.1.2.1 Complex I

In complex I, NADH is oxidized to NAD, ubiquinone (Q) is reduced to ubiquinol (QH_2), and four protons are transported into the IMS.

1.2.1.2.2 Complex II (succinate dehydrogenase)

In complex II, electrons from $FADH_2$ are transferred to Q resulting in QH_2. No protons are transported to the IMS.

1.2.1.2.3 Complex III

In complex III, QH_2 is oxidized while 2 molecules of cytochrome C (cyto C) are reduced and an additional four protons are transported into the IMS.

1.2.1.2.4 Complex IV

In complex IV, cyto C is oxidized, producing 2 molecules of water and transferring four protons to the IMS.

1.2.1.2.5 Complex V (F_oF_1-ATPase)

In complex V (F_oF_1-ATPase), energy from the proton gradient established by preceding complexes is utilized to phosphorylate ADP into ATP (Jonckheere et al., 2011).

1.2.1.2.6 ANT

ANT exchanges ADP and ATP across the IMM.

1.2.1.2.7 Phosphate translocase

Phosphate translocase (phosphate carrier), symports a phosphate ion and proton into the mitochondrial matrix from the IMS (Seifert et al., 2015).

1.2.1.3 ATP yield

Each original molecule of glucose theoretically yields the production of 40 ATP through the above detailed process. However, due to energy consumption required to support the process and transport of substrates the yield is lower: 2 molecules of ATP are consumed in glycolysis, pyruvate is actively transported into the IMS, ANT exchanges ADP (-3) with ATP (-4) across the IMM and which negates a portion of the generated of the proton motive force, and there is some leakage of protons from the IMS through the OMM. All of this together is believed to reduce the overall yield of the process to 28-30 net ATP molecules generated (Rich, 2003). It is not yet properly elucidated what portion of IMM potential is lost (or transferred) to the OMM which results and lowered ATP yield during respiration, and how various membrane control mechanisms influence this result. Tying together experimental results and theoretical predictions from modeling provides a path to further understanding these underlying mechanisms.

1.2.2 Substrate transport

As noted in the previous section, the IMM has specialized transporters and process to move metabolites, substrates and products to and from the mitochondrial matrix, while VDAC is the only mode of transport on the OMM. The major transporters of the IMM are overviewed presented in Figure 16 and include the potassium-hydrogen antiporter (KHE), sodium-hydrogen exchange (NHE), calcium-hydrogen exchange (CHE), sodium-calcium exchange (NCE), calcium uniporter (MCU), and the mitochondrial permeability transition pore (MPTP).

1.3 Bioenergetics concepts

This overviews key bioenergetics concepts which are utilized in this study to model VDAC and mitochondrial bioenergetics. The following section is derived from content and equations presented from the following references (Marco Colombini, 1994; Keener et al., 2009; S. V. Lemeshko et al., 2000; Palmeira et al., 2012).

1.3.1 Diffusion through membranes

The diffusion of substrates and ions across membranes (diffusion flux) is characterized by Fick's law which relates differences in concentration to diffusion flux.

$$\boldsymbol{J} = -D(\nabla c) \qquad \text{(Eq. 1)}$$

where,
$J = Diffusion\ flux$
$D = Fick's\ difussion\ constant$
$c = concentration\ of\ ionic\ species$

At steady state concentrations across membranes, the diffusion flux across a membrane can be expressed in the following form:

$$\boldsymbol{J} = -D(c_e - c_i) \qquad \text{(Eq. 2)}$$

1.3.2 Gibbs-Donnan equilibrium

The equilibrium resulting from charged particles diffusing through membranes is described by ***Donnan effect***. This equilibrium is driven by the fact that both chemical equilibrium and charges must be balanced on both side of the membrane. The equation below represents the characteristic constraint of the equilibrium.

$$[S']_e[S]_e = [S']_i[S]_i \qquad \text{(Eq. 3)}$$

where,
$[S] = concentration\ of\ (-)\ ionic\ species\ in\ external\ (e)\ and\ internal\ (i)\ compartments$
$[S'] = concentration\ of\ (+)\ ionic\ species\ in\ external\ (e)\ and\ internal\ (i)\ compartments$

The resulting potential from this equilibrium is described by the Nernst equation presented below.

1.3.3 Membrane potential

The permeability of substrates and ions across VDAC and the OMM is controlled through gating caused by changes in membrane potential. The primary governing equation which can be utilized to describe this relationship is the ***Nernst equation***, which establishes a relationship between the difference in ionic concentrations between membranes and the resulting potential difference.

$$V = \frac{RT}{zF}\ln\left(\frac{[S]_e}{[S]_i}\right) = \frac{kT}{zq}\ln\left(\frac{[S]_e}{[S]_i}\right) \qquad \text{(Eq. 4)}$$

where,

$$V = V_i - V_e \quad \text{(Eq. 5)}$$

Which represents the potential difference inside the membrane minus the potential difference outside (external to) the membrane *and,*

$R = gas\ constant$
$T = temperature$
$z = charge\ on\ ion$
$F = Faraday's\ constant$
$[S] = concentration\ of\ ionic\ species$
$k = \frac{R}{N_A}(Boltzmann's\ constant); where\ N_A = Avogadro's\ number$
$q = charge\ on\ proton$

To understand the flow of ions across the membrane, both contributions from concentration gradients as well as the electric field must be incorporated into the diffusion flux equation. This relationship expands upon Fick's law and is established by the ***Nernst-Plank equation.***

$$\boldsymbol{J} = -D\left(\nabla c + \frac{RT}{zF} c\nabla\phi\right) \quad \text{(Eq. 6)}$$

where,
$J = Diffusion\ flux$
$D = Fick's\ difussion\ constant$
$c = concentration\ of\ ionic\ species$
$\nabla\phi = electric\ field$

The solution to the Nernst-Plank equation requires knowledge of the electric field. If the electric field is assumed to be constant, a useful result to the Nernst-Plank equation is obtained. This result, obtained by Goldman, is known as the constant field approximation or the ***Goldman Hodgkin–Katz (GHK) equation***. The GHK equation for flux is presented below:

$$\boldsymbol{J} = \frac{D}{L}\frac{zF\nabla\phi}{RT}\left(\frac{C_e^{\frac{zFV}{RT}} - C_i}{e^{\frac{zFV}{RT}} - 1}\right) \quad \text{(Eq. 7)}$$

where,
$J = Diffusion\ flux$
$D = Fick's\ difussion\ constant$
$L = Membrane\ thickness$
$z = ionic\ charge$
$F = Faraday's\ constant$
$R = Gas\ constant$
$T = temperature$
$\nabla\phi = electric\ field$
$c = concentration\ of\ ionic\ species$

In addition to the flux form of the GHK equation presented above, the equation can also be modified into current form presented below, by multiplying by a factor of *zF*.

$$\boldsymbol{I} = \frac{D}{L}\frac{z^2F^2\nabla\phi}{RT}\left(\frac{C_e^{\frac{zFV}{RT}} - C_i}{e^{\frac{zFV}{RT}} - 1}\right) \quad \text{(Eq. 8)}$$

1.4 Bioenergetics modeling

This section aims to provide background into the motivation for the modeling methodologies utilized in this study, as well as reviewing key existing models of both VDAC and mitochondrial bioenergetics which this study aims to build on.

1.4.1 Modeling theory

1.4.1.1 Mechanistic modeling

The utility of a computational model for VDAC kinetics is twofold: (1) to study single channel behavior and (2) to integrate these kinetics into studies with other physiological processes. Empirically derived models (models derived based on data and observation) may be used to support the first type of study. However, in order to integrate the kinetics of VDAC into more comprehensive models of cellular processes (which is the aim herein) the developed

models should be designed based on applicable physical principles such as conservation of mass, charge, and energy (Beard, 2005).

1.4.1.2 Deterministic versus stochastic models

Deterministic models are ones in which the values of dependent variables in the target system can be fully computed through the inputs and parameters of the model. In deterministic modeling inherent variability and randomness within the system, if it is present, is not considered. Majority of deterministic approaches consist of models based on ordinary differential equations (ODEs). Solutions to ODE models are assisted by a wide breath of numerical methods and they are typically easier to form and analyze (Beard, 2005).

However, most biological systems and process are inherently random, and thus may be better represented by stochastic models. In stochastic modeling, dependent variables of a model are presented as probability distributions and the model outputs the likeliness of specific outcomes. While stochastic models may more accurately represent naturally occurring processes, they are difficult to formulate and analyze in comparison to deterministic approaches (Hahl et al., 2016).

1.4.2 Relevant VDAC computational models

1.4.2.1 Lemeshko et. al., 2000

Lemeshko et. al. present one of the earliest computational models of OMM potential generation and its effect on VDAC gating. Two models are presented: a simple membrane compartment model is presented demonstrating potential generation by an enzymatic reaction in KCl solution, and a more complex cellular model using phosphate ions which incorporates changes in permeability dependent on generated potential.

The compartment model simulates how metabolically driven potential can be generated when the permeability of reagents and products of chemical reactions differ across a membrane. This model is depicted in Figure 9 below, and involves anion A^- being converted by enzyme E into anion B^- within the membrane. The permeabilities of A, B and the salt solution of KCl each differ across the membrane, resulting in the generation of membrane potential as the reaction takes place. This result is described by Equation 9 below.

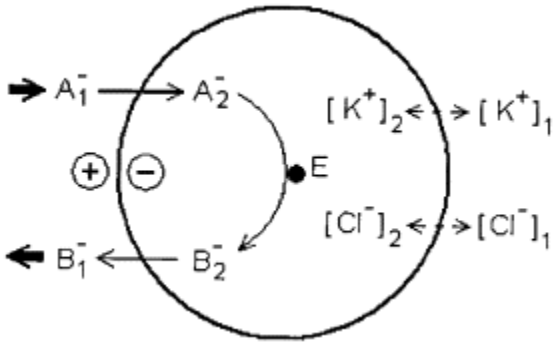

Figure 9: Compartment model of membrane potential generation (from S. V. Lemeshko et al., 2000)

$$V = \frac{RT}{F} \ln\left(\frac{[Cl]_1}{[Cl]_2}\right) \qquad \text{(Eq. 9)}$$

The cellular model (Figure 10A) simulates the generation of both Donnan and metabolic potential across the semi-permeable OMM. The model uses experimental data for phosphate ions and excludes nucleotides and salts for simplicity in analysis. The permeability of the ions is calculated as a function of the generated potential, and set to attenuate at high negative and positive potentials (Figure 10B).

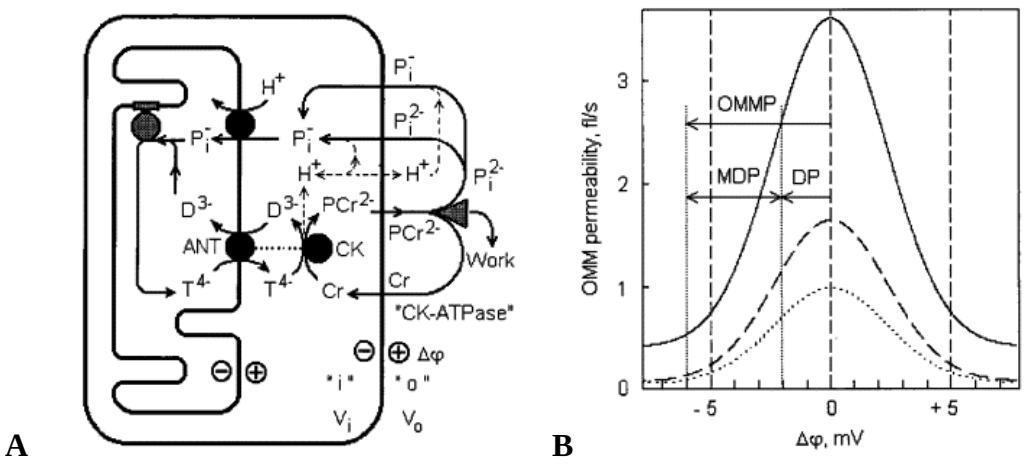

Figure 10: (A) Simple cellular model of OMM potential generation using phosphate ions. (B) Permeability – voltage relationship of phosphate ions (from S. V. Lemeshko et al., 2000)

The simulations of both models and resulting in non zero OMM potentials validate the possibility of membrane potential being generated across the mitochondrial OMM through both Donnan effects and as a result of metabolism in the IMM. The numerical outputs of the model are not physiologically relevant as only a small, nonrepresentative, subset IMM and OMM species are considered. However, the model is significant in establishing in the possibility of the phenomena on the mitochondrial OMM and its association with VDAC gating, providing a foundation for further investigation.

1.4.2.2 Tewari et. al, 2014

Tewari, et. al. presents a stochastic computational model of VDAC kinetics which investigates the impact of various PTMs using a Markov chain Monte Carlo (MCMC) method. In Markov chain models, the probability of each subsequent state in the modeled system depends on its past state. The model classifies various states of VDAC as open (O), intermediate or sub-states (O_s), and closed (C) based on thresholding of current through the channel (Tewari et al., 2014). Below is an example of the how the model is formulated.

$$Ek = E(tk) = \begin{cases} O, \ if \ |Ik| > |IO|, \\ C, \ if \ |Ik| < |IC|, \\ O_s, \ otherwise \end{cases} \quad \text{(Eq. 10)}$$

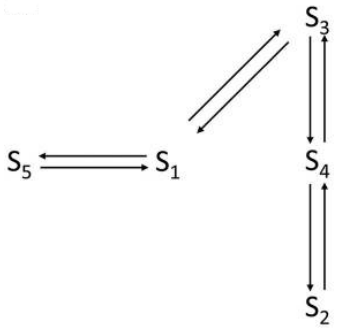

Figure 11: Markov model of VDAC states (from Tewari et al., 2014)

The states are defined as described previously, and current is segmented based on thresholds established for each state. Figure 11 is a representation of possible equilibrium model which could represent VDAC progression through various states. The study explores and contrasts kinetics through the proposed Markov chain of WT, nitrosated, and phosphorylated VDAC (Tewari et al., 2014). The study constraints its investigation to a constant applied membrane potential (-10 mV) through a single VDAC.

1.4.3 Relevant mitochondrial computational models

1.4.3.1 Beard, 2005

The first computer model of cellular respiration which is thermodynamically balanced and incorporates contributions from both chemical and electrical components was formulated by Beard. The model has three components: 1) electron transport chain (ETC) and oxidative phosphorylation, 2) cation transport across IMM, and 3) substrate transport across OMM which are depicted in the below graphic.

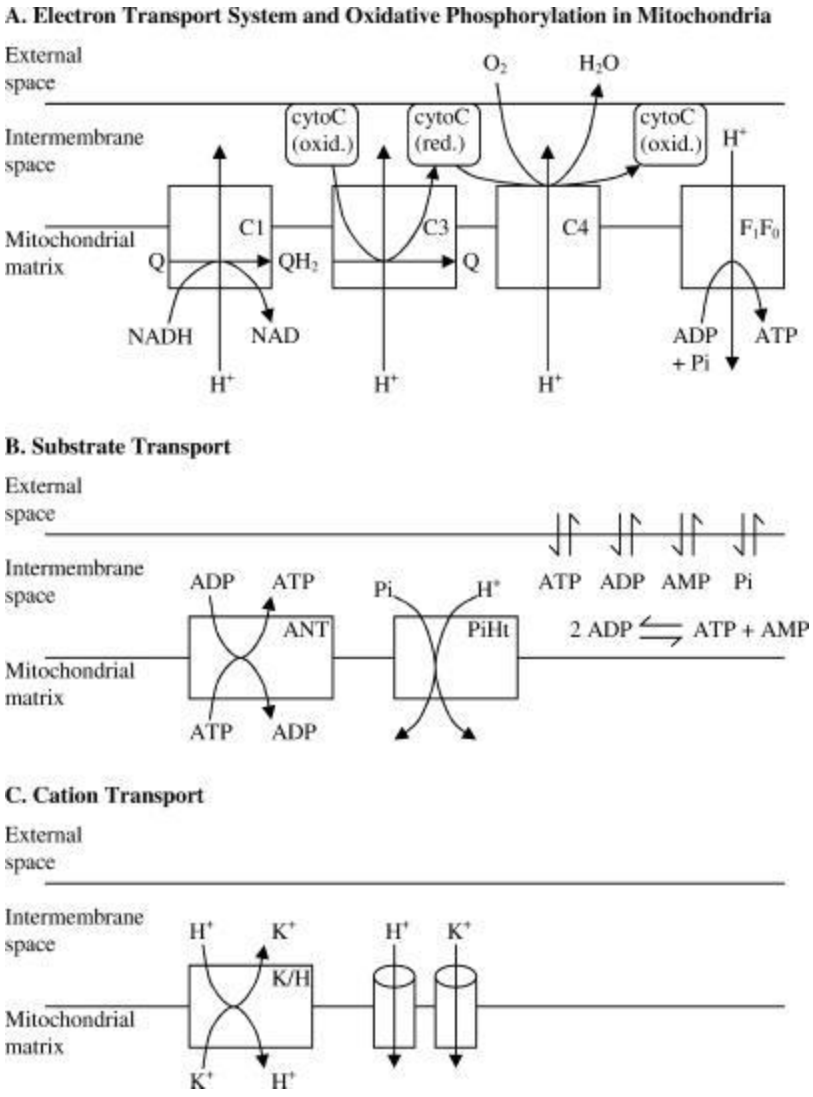

Figure 12: Components in Beard mitochondrial model (Beard, 2005)

Kinetic and mass balance equations were developed for each species incorporated in the model and parameterized based on fitting to experimentally available data and comparison to relevant datasets from Bose (Bose et al., 2003). The model conserves charge, mass, energy and is based on known physiological mechanisms. The model is governed by 17 ODEs representing each species-compartment and membrane potential on the inner membrane.

$$
\begin{aligned}
d[\mathrm{H}^+]_\mathrm{x}/dt &= \frac{1}{r_\mathrm{buff}}(-J_\mathrm{DH} - (4-1)J_\mathrm{C1} - (2+2)J_\mathrm{C3} \\
&\quad - (4-2)J_\mathrm{C4} + (n_A - 1)J_\mathrm{F1} \\
&\quad + 2J_\mathrm{PiHt} + J_\mathrm{Hle} - J_\mathrm{KH})/V_\mathrm{x} \\
d[\mathrm{K}^+]_\mathrm{x}/dt &= (+J_\mathrm{KH} + J_\mathrm{K})/V_\mathrm{x} \\
d[\mathrm{Mg}^{2+}]_\mathrm{x}/dt &= (-J_\mathrm{MgATPx} - J_\mathrm{MgADPx})/V_\mathrm{x} \\
d[\mathrm{NADH}]_\mathrm{x}/dt &= (+J_\mathrm{DH} - J_\mathrm{C1})/V_\mathrm{x} \\
d[\mathrm{QH_2}]_\mathrm{x}/dt &= (+J_\mathrm{C1} - J_\mathrm{C3})/V_\mathrm{x} \\
d[\mathrm{cytC(red)}^{2+}]_\mathrm{x}/dt &= (+2J_\mathrm{C3} - 2J_\mathrm{C4})/V_\mathrm{x} \\
d[\mathrm{ATP}]_\mathrm{x}/dt &= (+J_{\mathrm{F_1F_0}} - J_\mathrm{ANT})/V_\mathrm{x} \\
d[\mathrm{mATP}]_\mathrm{x}/dt &= (+J_\mathrm{MgATPx})/V_\mathrm{x} \\
d[\mathrm{mADP}]_\mathrm{x}/dt &= (+J_\mathrm{MgADPx})/V_\mathrm{x} \\
d[\mathrm{Pi}]_\mathrm{x}/dt &= (-J_{\mathrm{F_1F_0}} + J_\mathrm{PiHt})/V_\mathrm{x} \\
d[\mathrm{ATP}]_\mathrm{i}/dt &= (+J_\mathrm{ATPt} + J_\mathrm{ANT} + J_\mathrm{AKi})/V_\mathrm{i} \\
d[\mathrm{ADP}]_\mathrm{i}/dt &= (+J_\mathrm{ADPt} - J_\mathrm{ANT} - 2J_\mathrm{AKi})/V_\mathrm{i} \\
d[\mathrm{AMP}]_\mathrm{i}/dt &= (+J_\mathrm{AMPt} + J_\mathrm{AKi})/V_\mathrm{i} \\
d[\mathrm{mATP}]_\mathrm{i}/dt &= (+J_\mathrm{MgATPi})/V_\mathrm{i} \\
d[\mathrm{mADP}]_\mathrm{i}/dt &= (+J_\mathrm{MgADPi})/V_\mathrm{i} \\
d[\mathrm{Pi}]_\mathrm{i}/dt &= (+J_\mathrm{Pit} - J_\mathrm{PiHt})/V_\mathrm{i} \\
d\Delta\Psi/dt &= (4J_\mathrm{C1} + 2J_\mathrm{C3} + 4J_\mathrm{C4} - n_\mathrm{A}J_\mathrm{F1} \\
&\quad - J_\mathrm{ANT} - J_\mathrm{Hle} - J_\mathrm{K})/C_\mathrm{IM}
\end{aligned}
$$

Figure 13: Beard model governing equations (Beard, 2005)

The model is able to appropriately represent experimental data for complex I, complex IV, complex III, IMM pH changes, and IMM potential generation in isolated mitochondria at steady state and with ADP perturbations. These results are overviewed in Figure 14 below.

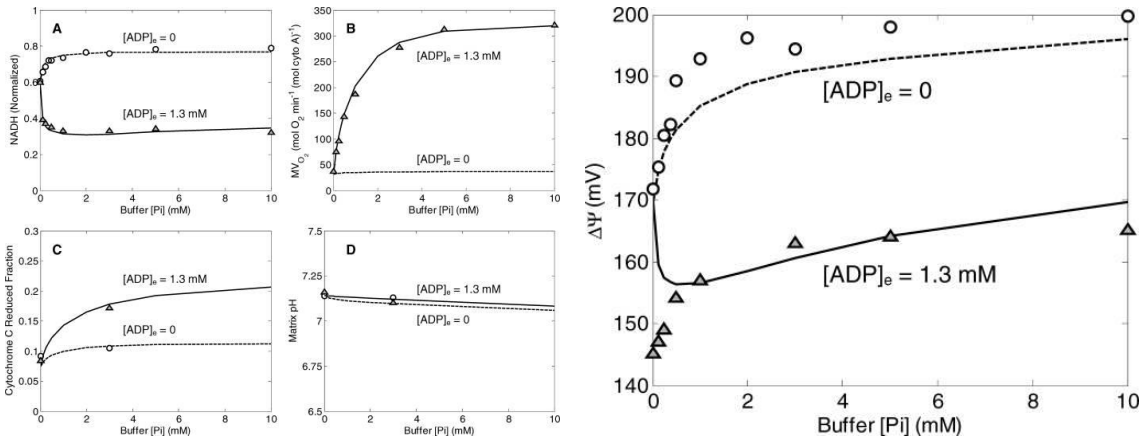

Figure 14: Beard model simulations and experimental data for complex I (A), complex IV (B), complex III (C), IMM pH (D), and IMM potential generation (E) (Beard, 2005)

The model offers a good representation of the major metabolites, reactions and components of the respiratory chain (OXPHOS and the ETC) on the IMM, the primary focus of its investigation. It does not attempt to characterize in detail the possible electrochemical affects based on OMM transport and channel and regulation. However, both due to its simplicity and completeness on formulating a functional IMM result, it is a good candidate to be utilized to study further components.

1.4.3.2 Wu, 2007

This model builds upon the previous models by Beard, with the key additions being an explicit TCA cycle, complex II, and additional IMM and OMM transport fluxes. The model is shown in Figure 8 in the previous section (Wu et al., 2007).

1.4.3.3 Dash and Beard, 2008

This model builds upon the previous model by Beard, with the addition of IMS transporters/exchangers for sodium and calcium (Dash et al., 2008).

1.4.4 Gaps in current understanding

As reviewed in this section, current computational models of mitochondrial function focus on IMM channels and reactions in the mitochondrial matrix. These models assume a

porous OMM, with minimal regulation, which is sufficient for the study and definition of many IMM and matrix processes at homeostasis. However proper understanding of OMM transport kinetics through VDAC can help define the interplay between OMM and IMM kinetics. This can be especially useful to study how various reactions and transport events impact IMM processes when influenced by various regulatory (or deregulatory) events.

Similarly, VDAC specific models reviewed in this section, and others proposed in literature, focus mainly on single channel bioenergetics. These models are powerful in understating and defining the function of the individual protein, but do not allow for broader investigations on its effects on other mitochondrial processes. Thus, the current gap in computation studies of both VDAC and mitochondria is integration of both of these layers.

2 Study Aims

**The results for studies overviewed in this section are presented in section 5 and organized in the same manner.*

2.1 Specific aim 1: Compute and integrate OMM (VDAC) transport fluxes and generated membrane potential into established mitochondrial function model

2.1.1 OMM potential generation

As proposed by the Lemeshko model, and postulated through numerous studies on VDAC function, the study will aim to demonstrate generation of OMM potential and characterize its effects the base model through the following comparisons.

2.1.2 IMM potential generation

The studies will investigate effects on IMM potential when OMM potential is accounted for, i.e. any effects or differences to steady-state potentials and potentials generated through ADP perturbations.

2.1.3 Oxygen consumption rate

The studies will show effects on oxygen consumption rate (through study of activity through complex IV) when accounting for OMM transport and potential at steady-state and through ADP perturbations.

2.1.4 NADH consumption and generation

The studies will show and changes in the consumption and generation rates of NADH when accounting for OMM transport and potential at steady-state and through ADP perturbations.

2.2 Specific aim 2: Simulate VDAC closure via addition of DIDS

As overviewed in section 1.1.7.2 DIDS can induce closure of VDAC. The effect of attenuation of permeability through the channel can be studied through the model generated in specific aim 1. This result will be compared with the following experimental data from the Dash lab.

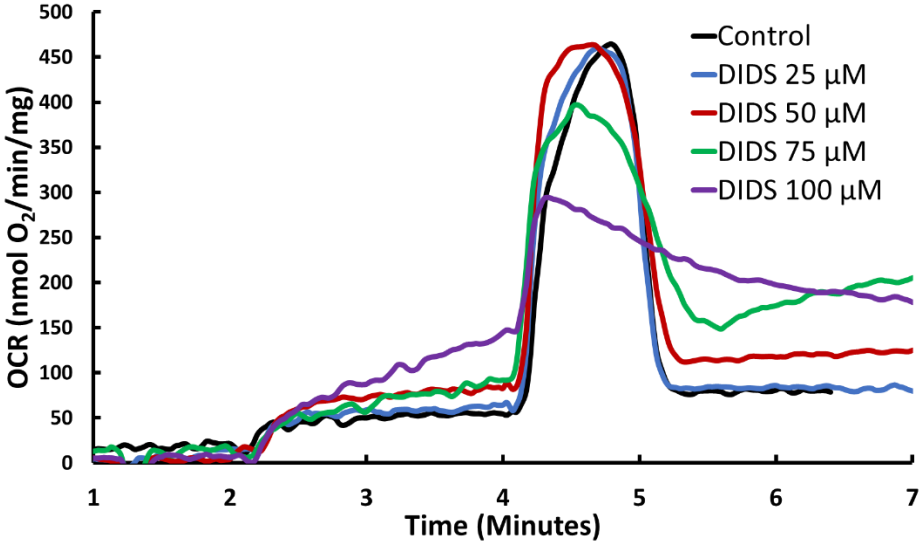

Figure 15: O2 consumption rate (OCR) at different concentration of VDAC inhibitor DIDS (generously provided by S. Kandel / Dash Lab, 2018, unpublished data)

3 Methods

3.1 Mitochondrial model

The computational mitochondrial function model overviewed in section 1.4.3.1 is used as a baseline and expanded to include VDAC function as described in the following section. The components of the base and expanded model are outlined in the below figure.

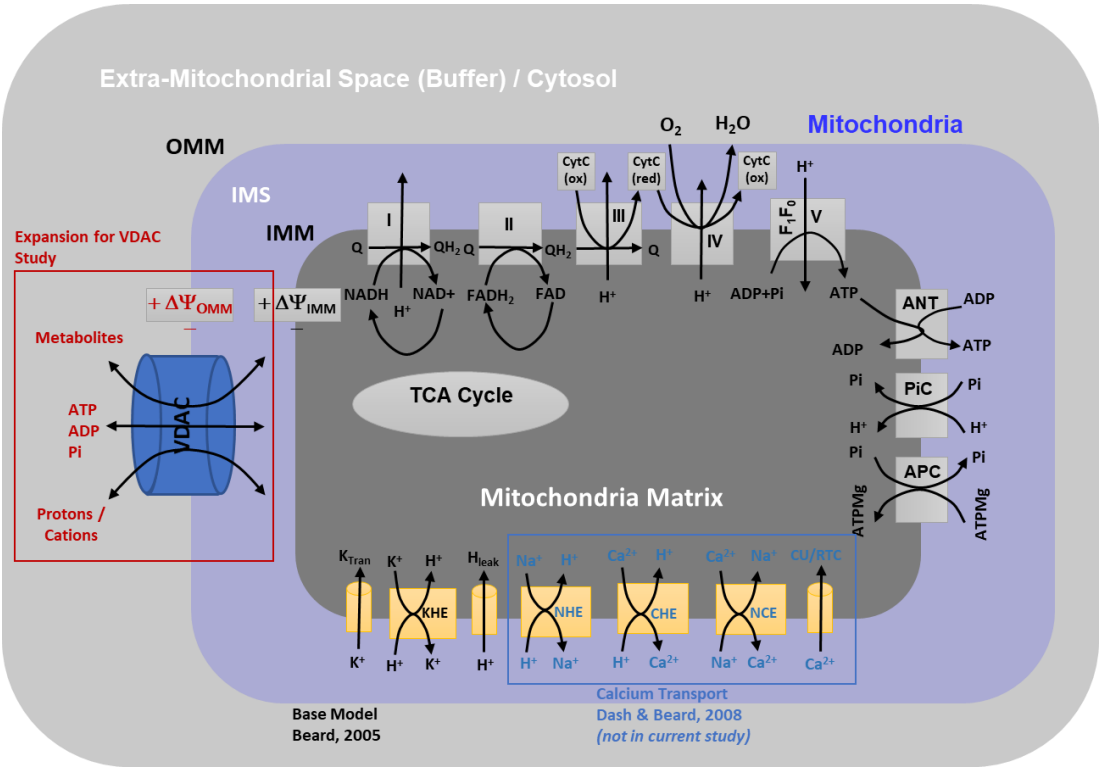

Figure 16: Cartoon representation of mitochondrial model from Dash group

3.2 OMM and VDAC specific equations

This section overviews variables/equations which are added to the above model to study OMM and VDAC behavior.

3.2.1 Permeation of key metabolites / substrates through VDAC

Flux through VDAC of key metabolites ATP, ADP, AMP and inorganic phosphate are described by the GHK flux equation introduced earlier and presented below for each species.

The GHK equation is used in the model where the OMM potential is not equal to zero. At zero potential the equation reduces to Fick's law and is modeled as such instead.

3.2.1.1 Anions

Permeation of ATP, ADP, AMP, phosphate and chlorine across the OMM is introduced into the model and governed through the following equations at nonzero potentials:

$$\boldsymbol{J_{ATP}} = \vartheta\gamma p_{ATP}\frac{-4F\nabla\phi_{OMM}}{RT}\left(\frac{[ATP]_e^{\frac{-4FV}{RT}}-[ATP]_i}{e^{\frac{-4FV}{RT}}-1}\right) \quad \text{(Eq. 11)}$$

$$\boldsymbol{J_{ADP}} = \vartheta\gamma p_{ADP}\frac{-3F\nabla\phi_{OMM}}{RT}\left(\frac{[ADP]_e^{\frac{-3FV}{RT}}-[ADP]_i}{e^{\frac{-3FV}{RT}}-1}\right) \quad \text{(Eq. 12)}$$

$$\boldsymbol{J_{AMP}} = \vartheta\gamma p_{AMP}\frac{-2F\nabla\phi_{OMM}}{RT}\left(\frac{[AMP]_e^{\frac{-2FV}{RT}}-[AMP]_i}{e^{\frac{-2FV}{RT}}-1}\right) \quad \text{(Eq. 13)}$$

$$\boldsymbol{J_{Pi}} = \vartheta\gamma p_{Pi}\frac{-F\nabla\phi_{OMM}}{RT}\left(\frac{[Pi]_e^{\frac{-FV}{RT}}-[Pi]_i}{e^{\frac{-FV}{RT}}-1}\right) \quad \text{(Eq. 14)}$$

$$\boldsymbol{J_{Cl}} = \vartheta\gamma p_{Cl}\frac{-F\nabla\phi_{OMM}}{RT}\left(\frac{[Cl]_e^{\frac{-FV}{RT}}-[Cl]_i}{e^{\frac{-FV}{RT}}-1}\right) \quad \text{(Eq. 15)}$$

The diffusion constant and membrane thickness paraments from equation 6 (D and L) are replaced here by permeability of each species (denote by $p_{species}$). An additional factor, γ, is added to normalize the flux to the mitochondrial volume. An additional factor of ϑ is included to represent open channel probability (described in section 3.2.4). The subscripts "e" and "i" denote concentrations of species in the cytosol and intermembrane space respectively. The fluxes are expressed in units of mass per unit time per liter mito volume (mol s^{-1} l mito vol^{-1}).

3.2.1.2 Cations

Proton and potassium fluxes are similarly introduced into the model and governed by the following equations:

$$\boldsymbol{J_{H_e}} = \gamma p_{H_e} \frac{F\nabla\phi_{OMM}}{RT}\left(\frac{[H]_e^{\frac{FV}{RT}} - [H]_i}{e^{\frac{FV}{RT}} - 1}\right) \quad \text{(Eq. 16)}$$

$$\boldsymbol{J_{K_e}} = \gamma p_{K_e} \frac{F\nabla\phi_{OMM}}{RT}\left(\frac{[K]_e^{\frac{FV}{RT}} - [K]_i}{e^{\frac{FV}{RT}} - 1}\right) \quad \text{(Eq. 17)}$$

The factor ϑ is not included as cations are not influenced by channel closure at high voltages in a similar manner to anions (Hodge et al., 1997).

3.2.2 OMM potential generation

Flux of charged metabolites through the outer membrane will result in the generation of a membrane potential. The generated potential can be described by the following relationship:

$$\frac{\boldsymbol{d\nabla\phi_{OMM}}}{\boldsymbol{dt}} = \frac{\left(-4J_{ATP} + -3J_{ADP} + -2J_{AMP} + -J_{Pi} + J_{H_e} + J_{K_e}\right)}{C_{OMM}} \quad \text{(Eq. 18)}$$

This potential incorporates both contributions from Donnan equilibrium between the cytosol and IMS to balance ionic charges, as well as metabolically derived potentials driven by the changes in metabolites and nucleotides from respiration in the inner membrane.

3.2.3 Parameter estimation

The parameters values used in the above equations are presented here.

Table 3. Parameter values for OMM equations

Name	Description	Value	Units	Reference	Equation
γ	Outer membrane area per liter mito volume	5.99	μm^{-1}	Beard (2005)	7-13
p_{ATP}	Permeability of OMM to ATP	327	$\mu m\ s^{-1}$		7
p_{ADP}	Permeability of OMM to ADP	327	$\mu m\ s^{-1}$		8
p_{AMP}	Permeability of OMM to AMP	327	$\mu m\ s^{-1}$		9
p_{Pi}	Permeability of OMM to phosphate	85	$\mu m\ s^{-1}$		10

p_{Cl}	Permeability of OMM to Cl	1e4	μm s^{-1}	-	11
p_{H_e}	Permeability of OMM to protons	1e7	μm s^{-1}	-	12
p_{K_e}	Permeability of OMM to potassium	1e4	μm s^{-1}	-	13
C_{OMM}	Capacitance of outer membrane	1e-7	mol (l mito volume)$^{-1}$ mV^{-1}	-	14

Values for γ, p_{ATP}, p_{ADP}, p_{AMP}, and p_{Pi} are used as is from the base model (Beard, 2005; Bose et al., 2003). Values for all other parameters were set as free parameters and are optimized to fit the model to experimental data.

3.2.4 Open channel probability

In order to account for attenuation of anion permeability as VDAC transitions between open and closed sets of stages based on changes in membrane potential, a factor for open channel probability depending on membrane potential is introduced and utilized in the model. This factor (or probability) is modeled off experimental data on the percent of VDACs on the OMM which are known to be open at varying voltages in a standard experimental medium (0.10 M KCl, 1.0 mM $CaCl_2$, 5.0 mM MES) simulating cytosolic behavior. The experimental results are presented below as reference for the empirically derived relationship.

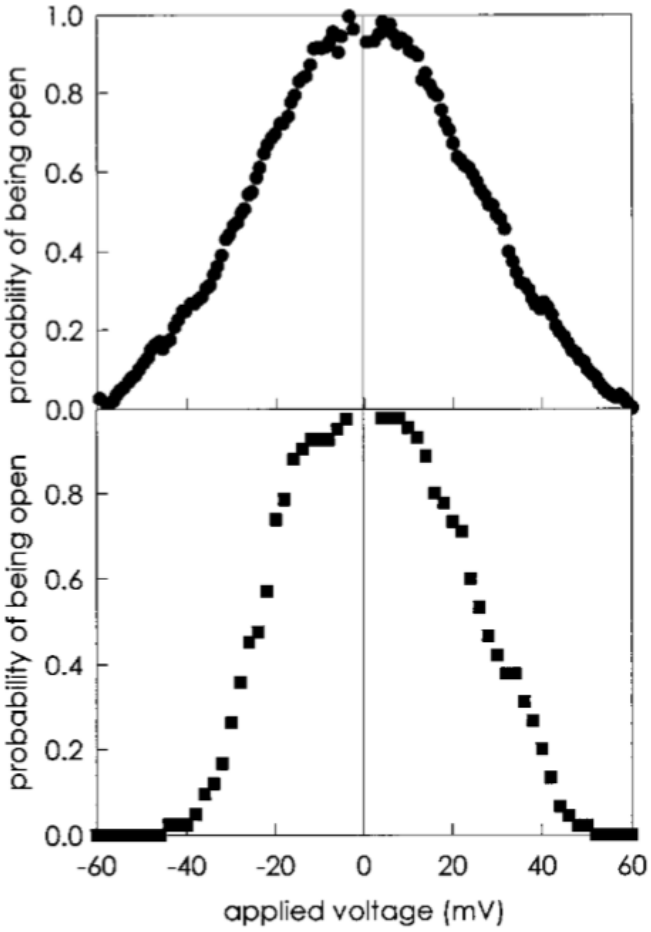

Figure 17: Voltage dependence on the conductance of VDAC (represented here as open channel probability) in standard mediums (Tatiana K. Rostovtseva et al., 1998)

The developed relationship is based on one presented by Lemeshko and coworkers which itself is a modification of the standard Gaussian formula.

Standard Gaussian Form:

$$f(x) = ae^{-\frac{(x-b)^2}{c^2}} \quad \text{(Eq. 10)}$$

Lemeshko and coworkers permeability-voltage dependance:

$$P = a_0[P_c + (P_0 - P_c)e^{-[ai\Delta\varphi+\delta)]^2}] \quad \text{(Eq. 11)}$$

$a_0 = absolute\ permeability\ coefficient$
$P_c = relative\ permeability\ (open)$
$P_0 = relative\ permeability\ (closed)$
$a = steepness\ coefficient$
$\Delta\varphi = membrane\ potential$
$\delta = membrane\ potential\ shift$

The gaussian model represents the probability density function for a normal variable. Eq. 11 puts this relationship in the context of permeability and voltage and adds modifications mainly to control the minimum and maximum outputs from the relationship (the independent relative closed probability term prevents the equation from zeroing out, and instead restricts the boundary to known physiological lower bounds). Motivated by the above relationships, similar equations are proposed to incorporate open channel probability into this model.

3.2.4.1 Gaussian model for membrane potential:

Motivated by the above relationships, the following relationship between open channel probability and membrane potential is proposed:

$$O(\Delta\varphi) = a + (b - a)e^{-c(\Delta\varphi - d)^2}$$

$O(\Delta\varphi) = open\ channel\ probability$
$a = minimum\ closed\ channel\ probability\ coefficient$
$b = maximum\ closed\ channel\ probability\ coefficient$
$c = steepness\ of\ descent\ coefficient$
$d = shift\ coefficient$
$\Delta\varphi = membrane\ potential$

The initial term (a + (b-a)) is utilized to properly bound the data to experimental observations (experimental min and max). The resulting fit of this equation to experimental data is presented below.

Fit Coefficients:
$a = 0$
$b = 1$
$c = 0.001137$
$d = -2.142$

Goodness-of-fit
sse: 0.2660
rsquare: 0.9684
dfe: 56
adjrsquare: 0.9679
rmse: 0.0689

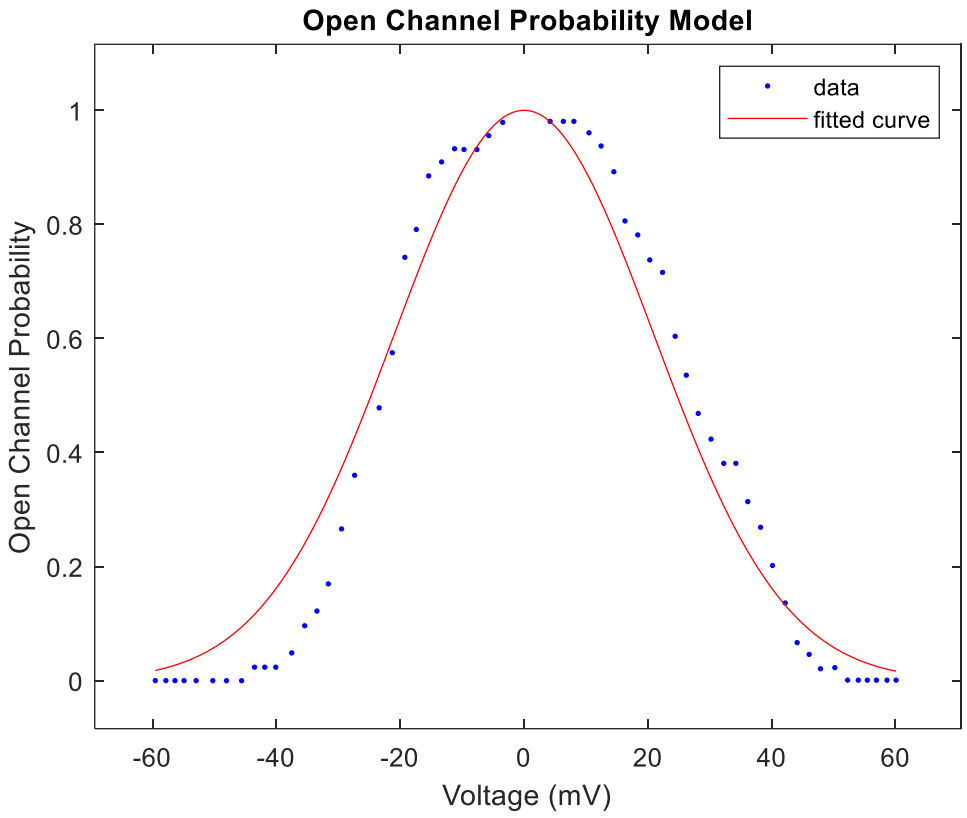

Figure 18: Standard gaussian model of open channel probability based on experimental data

While this fit is statistically decent, it poorly simulates certain key characteristics of our target: flatness observed in the data near the peak, the overall steepness of the data in attenuating open channels as potentials increase in either direction, and the rate at which the lower boundaries are reached on each of the tail ends. To attempt a better fit of these specific characteristic of the data, higher order gaussian models may be better suited.

3.2.4.2 Higher order gaussian model for membrane potential:

Based on the specific insufficiencies noted above, a higher order gaussian (super gaussian) model is instead utilized to simulate this relationship. This model is described below:

$$O(\Delta\varphi) = a + (b - a)e^{-c((\Delta\varphi - d)^2)^e}$$

$O(\Delta\varphi) = open\ channel\ probability$
$a = minimum\ closed\ channel\ probability\ coefficient$
$b = maximum\ closed\ channel\ probability\ coefficient$
$c = steepness\ of\ descent\ coefficient$
$d = shift\ coefficient$
e = power coefficient
$\Delta\varphi = membrane\ potential$

The power coefficient controls the order of the equation. Multiple higher orders were attempted (not shown) and power (e) coefficients between 1 and 2 were found to best represent the data (resulting in a overall power of ~2.8). The best resulting fit of this equation within acceptable bounds to experimental data is presented below. The error is significantly reduced, and this formulation additionally results in a better visual fit in regard to specific characteristics of the target system which we desire to model.

Fit Coefficients:
$a = 0.001$
$b = 1$
$c = 7e - 05$
$d = -2.2$
$e = 1.41$

Goodness-of-fit
sse: 0.0899
rsquare: 0.9893
dfe: 56
adjrsquare: 0.9889
rmse: 0.0401

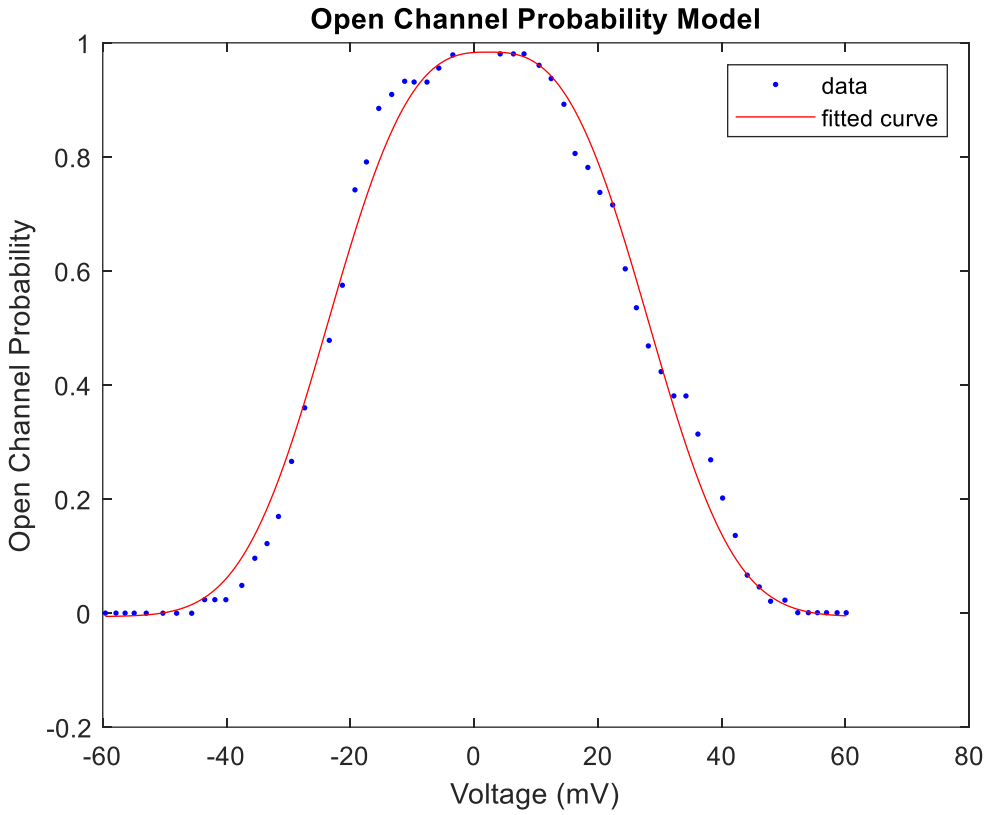
Open Channel Probability Model
data
fitted curve
Open Channel Probability
Voltage (mV)
1
0.8
0.6
0.4
0.2
0
-0.2
-60
-40
-20
0
20
40
60
80

3.3 Initial conditions

The following initial conditions (simulating isolated mitochondria in experimental buffer) were utilized for all simulations.

Table 4. Simulation initial conditions

Experimental conditions		
total CytC, Cred+Cox, molar	Ctot	2.70e-3
total Ubiquinol, Q+QH2, molar	Qtot	1.35e-3
total NAD+NADH, molar	NADtot	2.97e-3
total adenonucleotides, ATP+ADP, molar	Atot	10.0e-3
external pH	pH_e	7.15
IMS pH	pH_i	7.15
matrix pH	pH_x	7.2
Variables in original model		
inner membrane potential	dPsi	190
matrix proton concentration	H_x	10^(-pH_x)
matrix potassium concentration	K_x	140e-3
matrix NADH concentration	NADH_x	0.8*NADtot
matrix ubiquinol	Q	0.8*Qtot
Cyt C oxidase	Cox	0.8*Ctot
matrix oxygen	O2 (pO2 = 150 mmHg, alpha = 1.67e-6 M/mmHg, 25 oC)	250e-6
matrix ATP concentration	ATP_x	0.9*Atot
matrix ADP concentration	ADP_x	Atot-var(8)
inner membrane phosphate	Pi_x	5e-3
inner membrane ATP concentration	ATP_i	0
inner membrane ADP concentration	ADP_i	0
inner membrane AMP concentration	AMP_i	0
inner membrane phosphate concentration	Pi_i	5e-3
outer membrane ATP concentration	ATP_e	0
outer membrane ADP concentration	ADP_e	0
outer membrane AMP concentration	AMP_e	0
outer membrane phosphate concentration	Pi_e	5e-3
Variables added for OMM (VDAC) model		
outer membrane potential	dPSi_OMM	0
inner membrane proton concentration	IMS [H+], M	10^(-pH_i)
outer membrane proton concentration	external [H+], M	10^(-pH_e)
inner membrane potassium concentration	IMS [K+], M	140e-3

outer membrane potassium concentration	external [K+], M	140e-3
inner membrane chlorine concentration	Cl_i	135e-3
outer membrane chlorine concentration	Cl_e	135e-3

3.4 Simulation toolset

The model was developed, simulated and analyzed using MATLAB (version 9.5.0.944444, R2018b). Model codes are available from the Dash Lab upon request.

3.5 Simulation set-up

The following set-up was used to run model simulations:

Specific aim 1: All simulations were allowed to reach steady state (initial 30 seconds) and were then perturbated with 0.25 mM of ADP and again allowed to reach steady state. Run-time for all simulations was set to 400 seconds.

Specific aim 2: Model from specific aim 1 will be simulated at varying attenuated VDAC open channel probabilities (OP) to simulate blockage of channel with addition of DIDS to experimental medium.

4 Results

4.1 Specific aim 1: Compute and integrate OMM (VDAC) transport fluxes using GSK current equation into established mitochondrial function model

The derived equations (presented under methods) are incorporated into the model and utilized for the studies below.

4.1.1 OMM potential generation

The expanded model was simulated and allowed to reach steady state. No potential was observed to be generated on the OMM at steady state in the experimental medium. When the simulation was perturbed with ADP, the subsequent reactions and transport fluxes are shown to generate a minor potential difference across the OMM (Figure 19 below).

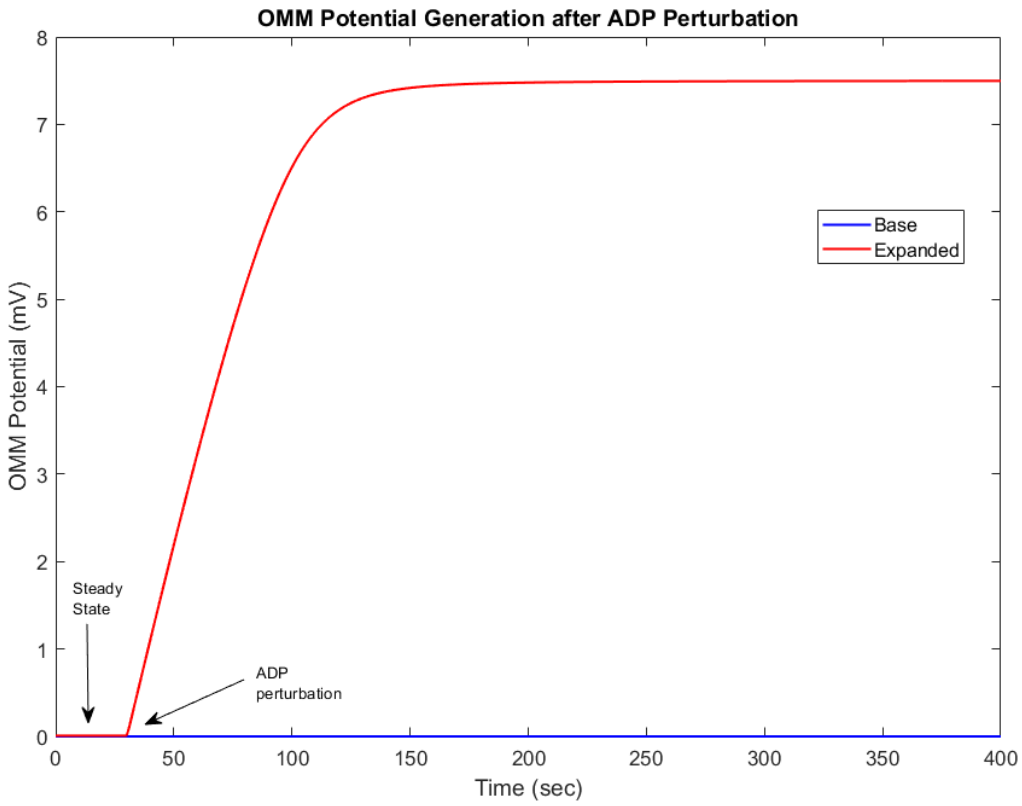

Figure 19: OMM potential generation after expansion of model to include VDAC kinetics

4.1.2 IMM potential generation

The simulation of the expanded model resulted in marked changes to IMM potential as compared to the base model. Subsequent to ADP perturbation, the both models result in a drop in membrane potential on the IMM. In the base model, membrane potential is immediately reestablished back to its steady state value. In the expanded model, however, the membrane potential continues to dip further (although at a lower rate) before being reestablished. The new steady-state established in the expanded model is lower than the initial steady-state.

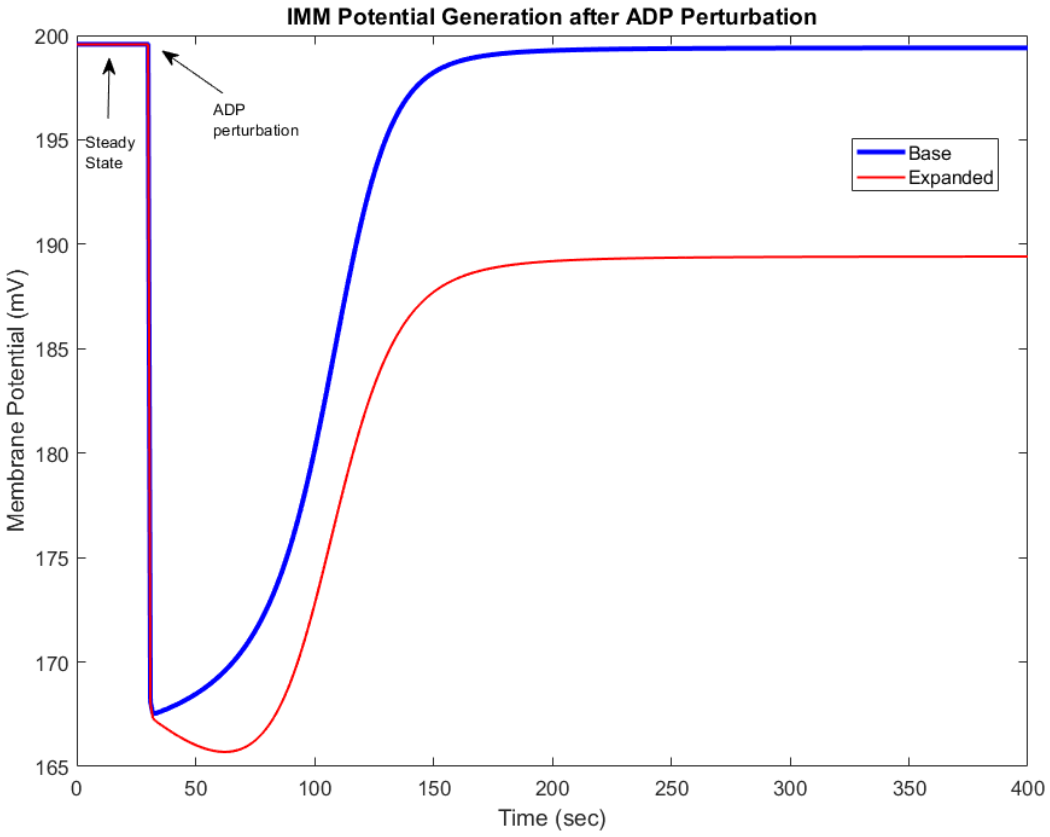

Figure 20: IMM potential generation before and after expansion of model to include VDAC kinetics

4.1.3 Oxygen consumption rate

Similar results are obtained for oxygen consumption through simulations of both base and expanded models. The reestablished steady-state rate in the expanded model is slightly elevated compared to the base model.

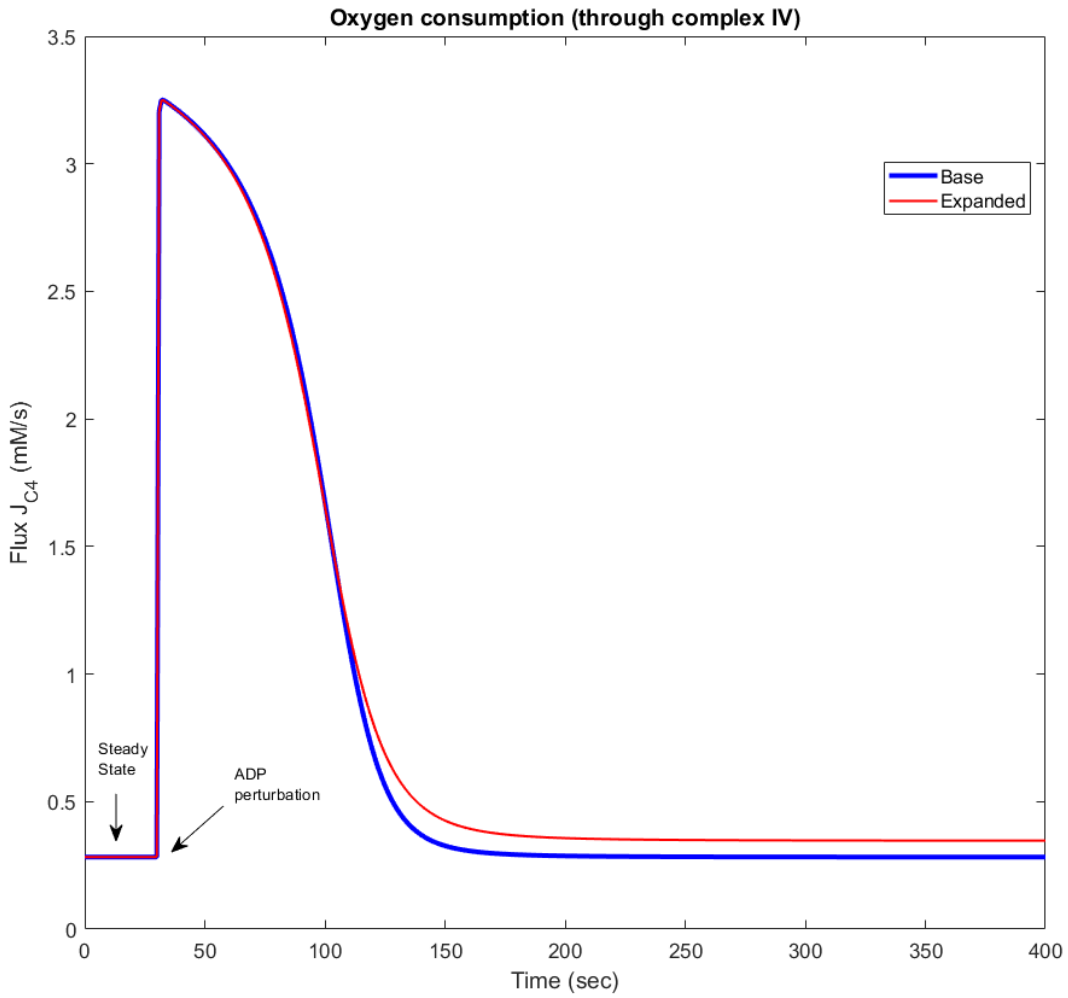

Figure 21: Oxygen consumption rate in base and expanded models

4.1.4 NADH consumption and generation

Simulations of both models result in similar behavior with respect to the equilibrium for matrix NADH and NAD^+. The expanded model reestablishes the equilibrium after ADP perturbation to a level slightly below the initial steady state, while the base model is able to fully reestablish equilibrium.

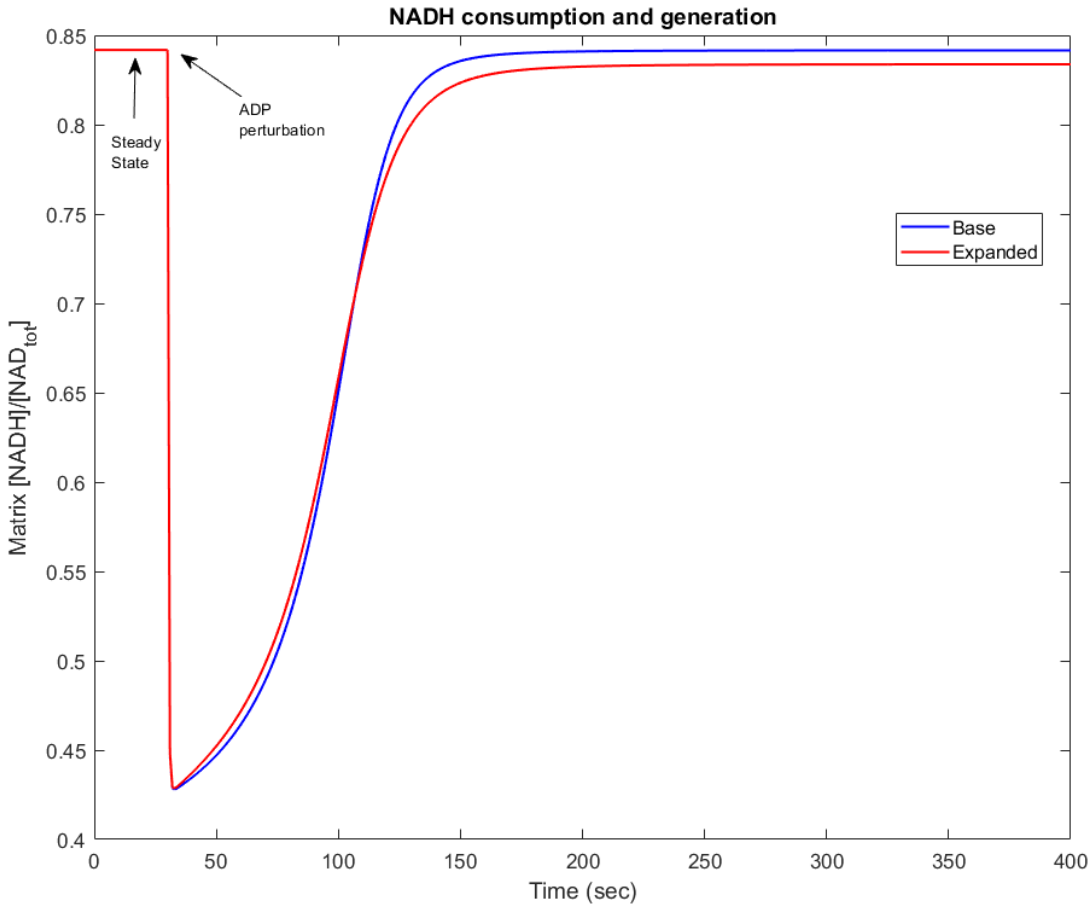

Figure 22: NADH consumption and generation in base and expanded models

4.2 Specific aim 2: Simulate VDAC closure via addition of DIDS

Peak oxygen consumption rates are shown to not be affected significantly with up to blockage of 50% of channels. Significant blockage of VDAC (open probabilities <10%) attenuate oxygen consumption rates. This is consistent with experimental data of VDAC blockage through DIDS presented in section 2.2.

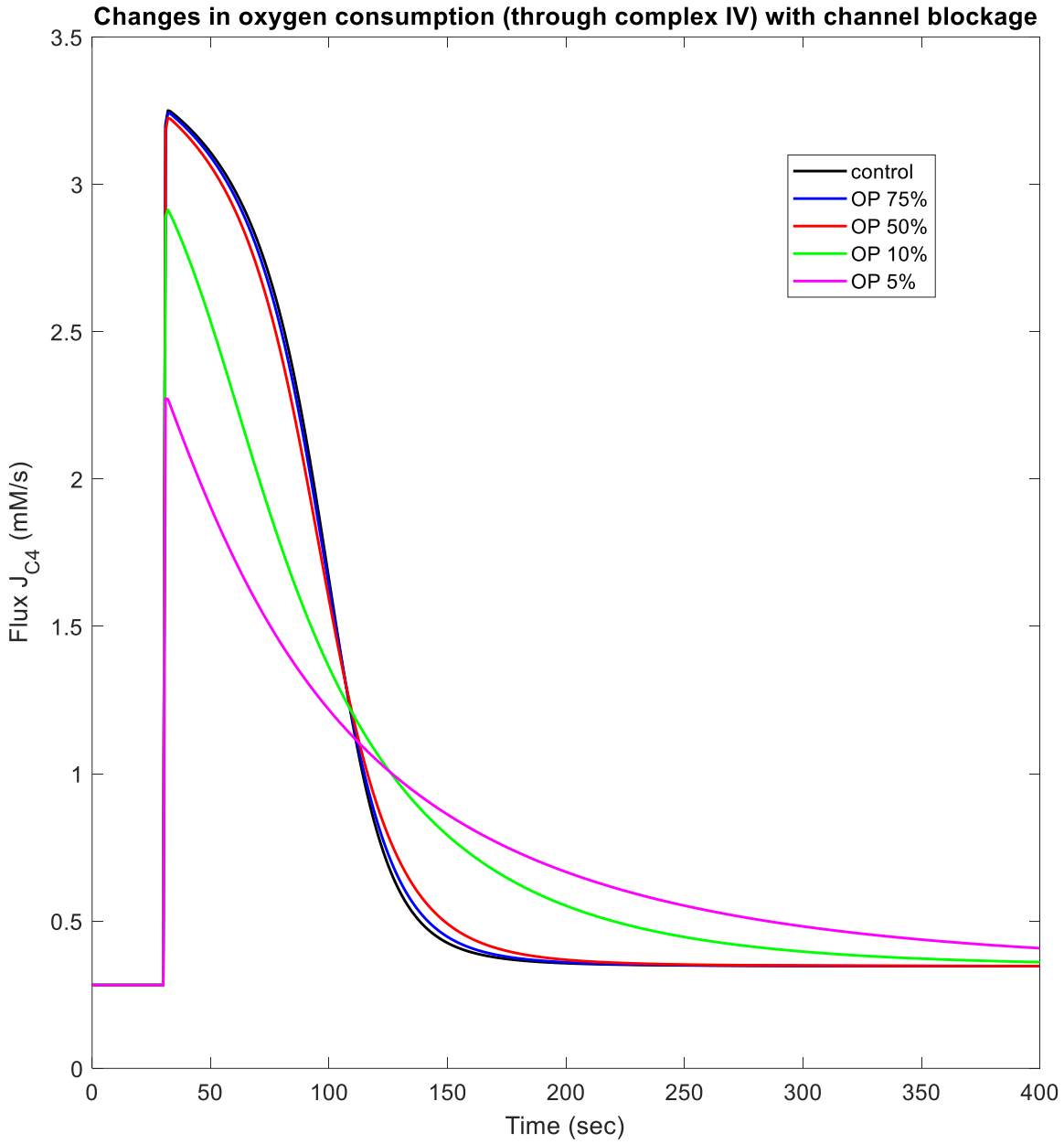

Figure 23: Changes due to complex IV flux (proxy for oxygen consumption rate) as VDACs are increasing blocked via reducing model parameter open channel probability (OP)

5 Discussion

5.1 Model development

The primary purpose of the study is to introduce a mechanistic model of transport through the OMM which accounts for VDAC kinetics. Transport of the main metabolically relevant anions (ATP, ADP, AMP and inorganic phosphate) were added to the model using GHK flux formulations to account for both chemical diffusion and electric field effects. The generated electric field (membrane potential) from this transport was calculated and used iteratively in the simulation to influence previously described transport fluxes. To account for observations in literature on how the properties of VDAC (namely opened / closed conformation resulting in altered permeability for anions) change with changes in potential additional parameters for "open probability" of the channel were introduced to properly attenuate substrate flux (and channel conductance). Model parameters are kept consistent with the base model where available or were otherwise based on literature and fit to experimental datasets. This expanded model of mitochondrial function to included VDAC kinetics should allow for broader study of interactions between the cytosolic, IMS and matrix environments during energy production as well as offer a mechanism to study regulatory events on the OMM.

5.2 Simulation outcomes

Simulations of the expanded isolated mitochondrial model after ADP perturbations result in the generation of an OMM potential as metabolites are consumed, and resulting products and ions are redistributed along their electrochemical gradients. The generation of OMM potential is consistent with previous computational studies by Lemeshko (see section 1.4.2.1) which, similar to this study, were able to demonstrate that both Donnan equilibrium and metabolically driven potentials can be generated following energy metabolism. A marked change from the base model

is observed with the IMM potential, which is attenuated after the introduction of an OMM potential. There is no available data in literature on the precise influences and differences between potentials across the IMM and OMM, so it is difficult to conclude if this is an accurate result or an unintended artifact of the model. Typically, measurements of "IMM" potential by fluorescence distinguish potential differences between the matrix and cytosol as the IMS space is too small to account for and measure against. As such, reported values of membrane potential (against which the base model was validated) can be attributed to either OMM or IMM potentials (Hu et al., 2008; Zorova et al., 2018). One possible explanation in support of this result is found in previous VDAC studies, which suggest IMM potential can be translocated to the OMM under certain conditions. However, these studies focus on niche mechanisms through IMM/OMM contact sites instead of steady-state energy metabolism (Benz et al., 1990; V. V. Lemeshko, 2002). In addition to the translocation of IMM potential to the OMM, the expanded model results in the slight total loss of membrane potential (2-3 mV) after ADP perturbations. This slight attenuation can be attributed to expected proton leak from the IMS through the OMM which was introduced in the model (whereas in the base model IMS and external pH was fixed).

Simulations of increasing VDAC closure in the model are comparable to experimental results from DIDS studies on isolated mitochondria, confirming that increase in channel blockage reduces peak oxygen consumption levels and impairs energy metabolism. However, the model suggests significant blockage (greater than 90% of VDAC channels on the OMM) is required to reduce complex IV activity and impair energy metabolism. This would imply that regulation of VDAC is an all or nothing event. Further experimental studies which are able to elucidate the association between the percent of channels blocked and oxygen consumption rates will be required to validate this result.

5.3 Future directions

One of the primary areas on which the base model can be expanded is through the incorporation of additional metabolite fluxes across the OMM and how these species influence on the cytosolic and IMS environments to impact VDAC properties. Specifically, calcium ions, for which IMS transport models already exist in the Dash lab, are of specific interest to model across the OMM to both better simulate potential generation and regulatory effects of calcium on VDAC (Dash et al., 2008; T. K. Rostovtseva et al., 2008).

In addition to substrates which transverse the membrane and participate in mitochondrial activity, modeling of protein interactions with VDAC is another key area into which the model may be expanded. Characterization of interactions with VDAC and each of the major regulatory proteins from the Bcl-2 family, hexokinase, and tubulin would allow for a more accurate picture of how membrane potential generation and changes modeled in this study influence overall mitochondrial behavior. Since these factors act independently of the electrostatic environment on which the model is driven (i.e. changes in metabolite fluxes and concentrations generating membrane potential), and instead alter the conformational state of VDAC they interact with the overall probability distribution will be affected. This may either attenuate the OMM potential generated through this preliminary model or subdue any changes which occur after perturbations of the model.

Beyond enhancements to the model useful to study mitochondrial bioenergetics, interactions between VDAC, hexokinase and DIDS can additionally be useful to study the underlying mechanisms behind the release of reactive oxygen species (ROS) from the mitochondrial matrix into the cytosol. ROS are required for energy production in the mitochondrial, but there release into the cellular environment leads to cytotoxicity. Therefore, ROS production and movement

needs to be tightly controlled by mitochondrial processes. It has been shown that VDAC is the main mediate of ROS release (Han et al., 2003). Overexpression of hexokinase prevents this release, and introduction of DIDS into the environment is also shown to block this release (Shoshan-Barmatz et al., 2010; Simamura et al., 2014). Both mechanisms are anti-apoptotic. Further study of these interactions may provide more insight into the regulation of ROS generation, movement within the cellular environment and their associated pro- and anti-apoptotic effects.

6 References

Review Articles

Colombini, M. (2012a). Mitochondrial outer membrane channels. *Chem Rev, 112*(12), 6373-6387. doi:10.1021/cr3002033

Colombini, M. (2012b). VDAC structure, selectivity, and dynamics. *Biochim Biophys Acta, 1818*(6), 1457-1465. doi:10.1016/j.bbamem.2011.12.026

De Pinto, V., Reina, S., Guarino, F., & Messina, A. (2008). Structure of the voltage dependent anion channel: state of the art. *Journal of Bioenergetics and Biomembranes, 40*(3), 139-147. doi:10.1007/s10863-008-9140-3

McCommis, K. S., & Baines, C. P. (2012). The role of VDAC in cell death: Friend or foe? *Biochimica et Biophysica Acta (BBA) - Biomembranes, 1818*(6), 1444-1450. doi:10.1016/j.bbamem.2011.10.025

Shoshan-Barmatz, V., De Pinto, V., Zweckstetter, M., Raviv, Z., Keinan, N., & Arbel, N. (2010). VDAC, a multi-functional mitochondrial protein regulating cell life and death. *Mol Aspects Med, 31*(3), 227-285. doi:10.1016/j.mam.2010.03.002

Texts

Colombini, M. (1994). Chapter 4 Anion Channels in the Mitochondrial Outer Membrane. In *Chloride Channels* (pp. 73-101).

Colombini, M., Blachly-Dyson, E., & Forte, M. (1996). VDAC, a channel in the outer mitochondrial membrane. *Ion Channels, 4*, 169-202. doi:10.1007/978-1-4899-1775-1_5

Fall, C. P. (2002). *Computational cell biology*. New York: Springer.

Keener, J., & Sneyd, J. (2009). *Mathematical Physiology* (2nd ed.).

Palmeira, C. M., & Moreno, A. J. (2012). *Mitochondrial Bioenergetics*.

Primary Research - VDAC Structure

Bayrhuber, M., Meins, T., Habeck, M., Becker, S., Giller, K., Villinger, S., . . . Zeth, K. (2008). Structure of the human voltage-dependent anion channel. *Proc Natl Acad Sci U S A, 105*(40), 15370-15375. doi:10.1073/pnas.0808115105

Choudhary, O. P., Paz, A., Adelman, J. L., Colletier, J. P., Abramson, J., & Grabe, M. (2014). Structure-guided simulations illuminate the mechanism of ATP transport through VDAC1. *Nat Struct Mol Biol, 21*(7), 626-632. doi:10.1038/nsmb.2841

Geula, S., Ben-Hail, D., & Shoshan-Barmatz, V. (2012). Structure-based analysis of VDAC1: N-terminus location, translocation, channel gating and association with anti-apoptotic proteins. *Biochem J, 444*(3), 475-485. doi:10.1042/BJ20112079

Hiller, S., Abramson, J., Mannella, C., Wagner, G., & Zeth, K. (2010). The 3D structures of VDAC represent a native conformation. *Trends Biochem Sci, 35*(9), 514-521. doi:10.1016/j.tibs.2010.03.005

Kahle, Philipp J., Tomasello, M. F., Guarino, F., Reina, S., Messina, A., & De Pinto, V. (2013). The Voltage-Dependent Anion Selective Channel 1 (VDAC1) Topography in the Mitochondrial Outer Membrane as Detected in Intact Cell. *PLoS One, 8*(12). doi:10.1371/journal.pone.0081522

Marques, E. J., Carneiro, C. M., Silva, A. S., & Krasilnikov, O. V. (2004). Does VDAC insert into membranes in random orientation? *Biochimica et Biophysica Acta (BBA) - Biomembranes, 1661*(1), 68-77. doi:10.1016/j.bbamem.2003.11.018

Ujwal, R., Cascio, D., Chaptal, V., Ping, P., & Abramson, J. (2014). Crystal packing analysis of murine VDAC1 crystals in a lipidic environment reveals novel insights on oligomerization and orientation. *Channels, 3*(3), 167-170. doi:10.4161/chan.3.3.9196

Ujwal, R., Cascio, D., Colletier, J. P., Faham, S., Zhang, J., Toro, L., . . . Abramson, J. (2008). The crystal structure of mouse VDAC1 at 2.3 A resolution reveals mechanistic insights into metabolite gating. *Proc Natl Acad Sci U S A, 105*(46), 17742-17747. doi:10.1073/pnas.0809634105

Primary Research - Modeling

Beard, D. A. (2005). A biophysical model of the mitochondrial respiratory system and oxidative phosphorylation. *PLoS Comput Biol, 1*(4), e36. doi:10.1371/journal.pcbi.0010036

Dash, R. K., & Beard, D. A. (2008). Analysis of cardiac mitochondrial Na+-Ca2+ exchanger kinetics with a biophysical model of mitochondrial Ca2+ handling suggests a 3:1 stoichiometry. *J Physiol, 586*(13), 3267-3285. doi:10.1113/jphysiol.2008.151977

Hahl, S. K., & Kremling, A. (2016). A Comparison of Deterministic and Stochastic Modeling Approaches for Biochemical Reaction Systems: On Fixed Points, Means, and Modes. *Frontiers in Genetics, 7*. doi:10.3389/fgene.2016.00157

Lemeshko, S. V., & Lemeshko, V. V. (2000). Metabolically derived potential on the outer membrane of mitochondria: a computational model. *Biophys J, 79*(6), 2785-2800. doi:10.1016/S0006-3495(00)76518-0

Lemeshko, V. V. (2002). Model of the Outer Membrane Potential Generation by the Inner Membrane of Mitochondria. *Biophysical Journal, 82*(2), 684-692. doi:10.1016/s0006-3495(02)75431-3

Tewari, S. G., Zhou, Y., Otto, B. J., Dash, R. K., Kwok, W. M., & Beard, D. A. (2014). Markov chain Monte Carlo based analysis of post-translationally modified VDAC gating kinetics. *Front Physiol, 5*, 513. doi:10.3389/fphys.2014.00513

Wu, F., Yang, F., Vinnakota, K. C., & Beard, D. A. (2007). Computer Modeling of Mitochondrial Tricarboxylic Acid Cycle, Oxidative Phosphorylation, Metabolite Transport, and Electrophysiology. *Journal of Biological Chemistry, 282*(34), 24525-24537. doi:10.1074/jbc.M701024200

Zambrowicz, E. B., & Colombini, M. (1993). Zero-current potentials in a large membrane channel: a simple theory accounts for complex behavior. *Biophys J, 65*(3), 1093-1100. doi:10.1016/S0006-3495(93)81148-2

Primary Research - VDAC Experimental Studies

Benz, R., Kottke, M., & Brdiczka, D. (1990). The cationically selective state of the mitochondrial outer membrane pore: a study with intact mitochondria and reconstituted mitochondrial porin. *Biochimica et Biophysica Acta (BBA) - Biomembranes, 1022*(3), 311-318. doi:10.1016/0005-2736(90)90279-w

Chen, Y., Craigen, W. J., & Riley, D. J. (2014). Nek1 regulates cell death and mitochondrial membrane permeability through phosphorylation of VDAC1. *Cell Cycle, 8*(2), 257-267. doi:10.4161/cc.8.2.7551

Colombini, M. (1979). A candidate for the permeability pathway of the outer mitochondrial membrane. *Nature, 279*(5714), 643-645. doi:10.1038/279643a0

Colombini, M. (1980). Structure and mode of action of a voltage dependent anion-selective channel (VDAC) located in the outer mitochondrial membrane. *Ann N Y Acad Sci, 341*, 552-563. doi:10.1111/j.1749-6632.1980.tb47198.x

Crompton, M. (1999). The mitochondrial permeability transition pore and its role in cell death. *Biochemical Journal, 341*(2), 233-249. doi:10.1042/bj3410233

De Pinto, V., Messina, A., Accardi, R., Aiello, R., Guarino, F., Tomasello, M. F., . . . Lawen, A. (2003). New functions of an old protein: the eukaryotic porin or voltage dependent anion selective channel (VDAC). *Ital J Biochem, 52*(1), 17-24. Retrieved from https://www.ncbi.nlm.nih.gov/pubmed/12833633

Gonzalez-Gronow, M., Kalfa, T., Johnson, C. E., Gawdi, G., & Pizzo, S. V. (2003). The Voltage-dependent Anion Channel Is a Receptor for Plasminogen Kringle 5 on Human Endothelial Cells. *Journal of Biological Chemistry, 278*(29), 27312-27318. doi:10.1074/jbc.M303172200

Han, D., Antunes, F., Canali, R., Rettori, D., & Cadenas, E. (2003). Voltage-dependent Anion Channels Control the Release of the Superoxide Anion from Mitochondria to Cytosol. *Journal of Biological Chemistry, 278*(8), 5557-5563. doi:10.1074/jbc.M210269200

Hodge, T., & Colombini, M. (1997). Regulation of metabolite flux through voltage-gating of VDAC channels. *J Membr Biol, 157*(3), 271-279. doi:10.1007/s002329900235

Lee, A.-C., Xu, X., & Colombini, M. (1996). The Role of Pyridine Dinucleotides in Regulating the Permeability of the Mitochondrial Outer Membrane. *Journal of Biological Chemistry, 271*(43), 26724-26731. doi:10.1074/jbc.271.43.26724

Liu, A.-H., Cao, Y.-N., Liu, H.-T., Zhang, W.-W., Liu, Y., Shi, T.-W., . . . Wang, X.-M. (2008). DIDS Attenuates Staurosporine-induced Cardiomyocyte Apoptosis by PI3K/Akt Signaling Pathway: Activation of eNOS/NO and Inhibition of Bax Translocation. *Cellular Physiology and Biochemistry, 22*(1-4), 177-186. doi:10.1159/000149795

Mannella, C. A., & Guo, X. W. (1990). Interaction between VDAC channel and a polyanionic effector. An electron microscopic study. *Biophysical Journal, 57*(1), 23-31. doi:10.1016/s0006-3495(90)82503-0

Neumann, D., Bückers, J., Kastrup, L., Hell, S. W., & Jakobs, S. (2010). Two-color STED microscopy reveals different degrees of colocalization between hexokinase-I and the three human VDAC isoforms. *PMC Biophysics, 3*(1). doi:10.1186/1757-5036-3-4

Rostovtseva, T., & Colombini, M. (1997). VDAC channels mediate and gate the flow of ATP: implications for the regulation of mitochondrial function. *Biophys J, 72*(5), 1954-1962. doi:10.1016/S0006-3495(97)78841-6

Rostovtseva, T. K., & Bezrukov, S. M. (1998). ATP Transport Through a Single Mitochondrial Channel, VDAC, Studied by Current Fluctuation Analysis. *Biophysical Journal, 74*(5), 2365-2373. doi:10.1016/s0006-3495(98)77945-7

Rostovtseva, T. K., & Bezrukov, S. M. (2008). VDAC regulation: role of cytosolic proteins and mitochondrial lipids. *J Bioenerg Biomembr, 40*(3), 163-170. doi:10.1007/s10863-008-9145-y

Rostovtseva, T. K., Kazemi, N., Weinrich, M., & Bezrukov, S. M. (2006). Voltage Gating of VDAC Is Regulated by Nonlamellar Lipids of Mitochondrial Membranes. *Journal of Biological Chemistry, 281*(49), 37496-37506. doi:10.1074/jbc.M602548200

Rostovtseva, T. K., Komarov, A., Bezrukov, S. M., & Colombini, M. (2002). VDAC channels differentiate between natural metabolites and synthetic molecules. *J Membr Biol, 187*(2), 147-156. doi:10.1007/s00232-001-0159-1

Rostovtseva, T. K., Petrache, H. I., Kazemi, N., Hassanzadeh, E., & Bezrukov, S. M. (2008). Interfacial Polar Interactions Affect Gramicidin Channel Kinetics. *Biophysical Journal, 94*(4), L23-L25. doi:10.1529/biophysj.107.120261

Shimizu, S., Narita, M., & Tsujimoto, Y. (1999). Bcl-2 family proteins regulate the release of apoptogenic cytochrome c by the mitochondrial channel VDAC. *Nature, 399*(6735), 483-487. doi:10.1038/20959

Tan, W., & Colombini, M. (2007). VDAC closure increases calcium ion flux. *Biochimica et Biophysica Acta (BBA) - Biomembranes, 1768*(10), 2510-2515. doi:10.1016/j.bbamem.2007.06.002

Vander Heiden, M. G., Chandel, N. S., Li, X. X., Schumacker, P. T., Colombini, M., & Thompson, C. B. (2000). Outer mitochondrial membrane permeability can regulate coupled respiration and cell survival. *Proc Natl Acad Sci U S A, 97*(9), 4666-4671. doi:10.1073/pnas.090082297

Vander Heiden, M. G., Chandel, N. S., Williamson, E. K., Schumacker, P. T., & Thompson, C. B. (1997). Bcl-xL Regulates the Membrane Potential and Volume Homeostasis of Mitochondria. *Cell, 91*(5), 627-637. doi:10.1016/s0092-8674(00)80450-x

Xu, X., Forbes, J. G., & Colombini, M. (2001). Actin Modulates the Gating of Neurospora crassa VDAC. *Journal of Membrane Biology, 180*(1), 73-81. doi:10.1007/s002320010060

Zizi, M., Byrd, C., Boxus, R., & Colombini, M. (1998). The Voltage-Gating Process of the Voltage-Dependent Anion Channel Is Sensitive to Ion Flow. *Biophysical Journal, 75*(2), 704-713. doi:10.1016/s0006-3495(98)77560-5

Primary Research - VDAC Pathology

Das, S., Steenbergen, C., & Murphy, E. (2012). Does the voltage dependent anion channel modulate cardiac ischemia-reperfusion injury? *Biochim Biophys Acta, 1818*(6), 1451-1456. doi:10.1016/j.bbamem.2011.11.008

Fang, D., & Maldonado, E. N. (2018). VDAC Regulation: A Mitochondrial Target to Stop Cell Proliferation. In (pp. 41-69).

Kerner, J., Lee, K., Tandler, B., & Hoppel, C. L. (2012). VDAC proteomics: Post-translation modifications. *Biochimica et Biophysica Acta (BBA) - Biomembranes, 1818*(6), 1520-1525. doi:10.1016/j.bbamem.2011.11.013

Saks, V., Guzun, R., Timohhina, N., Tepp, K., Varikmaa, M., Monge, C., . . . Seppet, E. (2010). Structure–function relationships in feedback regulation of energy fluxes in vivo in health and disease: Mitochondrial Interactosome. *Biochimica et Biophysica Acta (BBA) - Bioenergetics, 1797*(6-7), 678-697. doi:10.1016/j.bbabio.2010.01.011

Schwertz, H., Carter, J. M., Abdudureheman, M., Russ, M., Buerke, U., Schlitt, A., . . . Buerke, M. (2007). Myocardial ischemia/reperfusion causes VDAC phosphorylation which is reduced by cardioprotection with a p38 MAP kinase inhibitor. *Proteomics, 7*(24), 4579-4588. doi:10.1002/pmic.200700734

Shoshan-Barmatz, V., & Mizrachi, D. (2012). VDAC1: from structure to cancer therapy. *Front Oncol, 2*, 164. doi:10.3389/fonc.2012.00164

Simamura, E., Hirai, K.-I., Shimada, H., Koyama, J., Niwa, Y., & Shimizu, S. (2014). Furanonaphthoquinones cause apoptosis of cancer cells by inducing the production of

reactive oxygen species by the mitochondrial voltage-dependent anion channel. *Cancer Biology & Therapy, 5*(11), 1523-1529. doi:10.4161/cbt.5.11.3302

Yuan, S., Fu, Y., Wang, X., Shi, H., Huang, Y., Song, X., . . . Luo, Y. (2008). Voltage-dependent anion channel 1 is involved in endostatin-induced endothelial cell apoptosis. *The FASEB Journal, 22*(8), 2809-2820. doi:10.1096/fj.08-107417

Primary Research - Other

Bose, S., French, S., Evans, F. J., Joubert, F., & Balaban, R. S. (2003). Metabolic Network Control of Oxidative Phosphorylation. *Journal of Biological Chemistry*, *278*(40), 39155-39165. doi:10.1074/jbc.M306409200

Hu, J., Dong, L., & Outten, C. E. (2008). The Redox Environment in the Mitochondrial Intermembrane Space Is Maintained Separately from the Cytosol and Matrix. *Journal of Biological Chemistry, 283*(43), 29126-29134. doi:10.1074/jbc.M803028200

Jonckheere, A. I., Smeitink, J. A. M., & Rodenburg, R. J. T. (2011). Mitochondrial ATP synthase: architecture, function and pathology. *Journal of Inherited Metabolic Disease, 35*(2), 211-225. doi:10.1007/s10545-011-9382-9

Rich, P. R. (2003). The molecular machinery of Keilin's respiratory chain. *Biochemical Society Transactions, 31*(6), 1095-1105. doi:10.1042/bst0311095

Seifert, E. L., Ligeti, E., Mayr, J. A., Sondheimer, N., & Hajnóczky, G. (2015). The mitochondrial phosphate carrier: Role in oxidative metabolism, calcium handling and mitochondrial disease. *Biochemical and Biophysical Research Communications, 464*(2), 369-375. doi:10.1016/j.bbrc.2015.06.031

Zorova, L. D., Popkov, V. A., Plotnikov, E. Y., Silachev, D. N., Pevzner, I. B., Jankauskas, S. S., . . . Zorov, D. B. (2018). Mitochondrial membrane potential. *Analytical Biochemistry, 552*, 50-59. doi:10.1016/j.ab.2017.07.009

7 Appendix

7.1 Endnote databases

This database contains all review and primary research articles cited herein and physical copies of these works where permissible. It is provided for utilization in future works on this topic.